Optimization under uncertainty of a hybrid waste tire and natural gas feedstock flexible polygeneration system using a decomposition algorithm

Authors:

Avinash Subramanian, Rohit Kannan, Flemming Holtorf, Thomas A. Adams II, Truls Gundersen, Paul I. Barton

Date Submitted: 2022-04-05

Keywords: Polygeneration system, Waste-to-Energy, Stochastic Programming, Decomposition Algorithm, Waste Tire, Optimization under uncertainty

Abstract:

Market uncertainties motivate the development of flexible polygeneration systems that are able to adjust operating conditions to favor production of the most profitable product portfolio. However, this operational flexibility comes at the cost of higher capital expenditure. A scenario-based two-stage stochastic nonconvex Mixed-Integer Nonlinear Programming (MINLP) approach lends itself naturally to optimizing these trade-offs. This work studies the optimal design and operation under uncertainty of a hybrid feedstock flexible polygeneration system producing electricity, methanol, dimethyl ether, olefins or liquefied (synthetic) natural gas. The recently developed GOSSIP software framework is used for modeling the optimization problem as well as its efficient solution using the Nonconvex Generalized Benders Decomposition (NGBD) algorithm. Two different cases are studied: The first uses estimates of the means and variances of the uncertain parameters from historical data, whereas the second assesses the impact of increased uncertain parameter volatility. The value of implementing flexible designs characterized by the value of the stochastic solution (VSS) is in the range of 260 - 405 M$ for a scale of approximately 893 MW of thermal input. Increased price volatility around the same mean results in higher expected net present value and VSS as operational flexibility allows for asymmetric exploitation of price peaks.

Record Type: Preprint

Submitted To: LAPSE (Living Archive for Process Systems Engineering)

Citation (overall record, always the latest version):	LAPSE:2021.0798
Citation (this specific file, latest version):	LAPSE:2021.0798-1
Citation (this specific file, this version):	LAPSE:2021.0798-1v2

Optimization under uncertainty of a hybrid waste tire and natural gas feedstock flexible polygeneration system using a decomposition algorithm

Avinash S.R. Subramanian[a], Rohit Kannan[b], Flemming Holtorf[c], Thomas A. Adams II[d], Truls Gundersen[a], Paul I. Barton[c]

[a]*Department of Energy and Process Engineering, Norwegian University of Science and Technology (NTNU), Kolbjørn Hejes vei 1B, NO-7491, Trondheim, Norway.*
[b]*Center for Nonlinear Studies and Theoretical Division (T-5), Los Alamos National Laboratory, Los Alamos, NM 87545 USA.*
[c]*Process Systems Engineering Laboratory, Department of Chemical Engineering, Massachusetts Institute of Technology, 77 Massachusetts Avenue, Cambridge, Massachusetts 02139, United States.*
[d]*Department of Chemical Engineering, McMaster University, 1280 Main St. W, Hamilton, ON, Canada, L8S 4L7.*

Abstract

Market uncertainties motivate the development of flexible polygeneration systems that are able to adjust operating conditions to favor production of the most profitable product portfolio. However, this operational flexibility comes at the cost of higher capital expenditure. A scenario-based two-stage stochastic nonconvex Mixed-Integer Nonlinear Programming (MINLP) approach lends itself naturally to optimizing these trade-offs. This work studies the optimal design and operation under uncertainty of a hybrid feedstock flexible polygeneration system producing electricity, methanol, dimethyl ether, olefins or liquefied (synthetic) natural gas. The recently developed GOSSIP software framework is used for modeling the optimization problem as well as its efficient solution using the Nonconvex Generalized Benders Decomposition (NGBD) algorithm. Two different cases are studied: The first uses estimates of the means and variances of the uncertain parameters from historical data, whereas the second assesses the impact of increased uncertain parameter volatility. The value of implementing flexible designs characterized by the value of the stochastic solution (VSS) is in the range of 260 - 405 M$ for a scale of approximately 893 MW of thermal input. Increased price volatility around the same mean results in higher expected net present value

and VSS as operational flexibility allows for asymmetric exploitation of price peaks.

Keywords: Polygeneration system, Waste-to-Energy, Stochastic Programming, Decomposition Algorithm, Waste Tire, Optimization under uncertainty

1. Introduction

Polygeneration involves the production of multiple products such as a mix of electricity, fuels (gasoline, diesel, synthetic natural gas, hydrogen) and chemicals (methanol, dimethyl ether, olefins, acetic acid) in the same location. One pertinent strategy is to also use multiple complementary feedstocks in order to exploit certain synergies, for instance, by generating syngas of different qualities that can be blended to provide the correct H_2/CO ratio for downstream synthesis, sharing of upstream equipment or heat integration of exothermic and endothermic processing units [1, 2]. In addition, including an alternative feedstock such as waste tire [3, 4], plastics, municipal solid waste [5] or petcoke [6, 7] may allow energy companies to lower their overall environmental impact while also mitigating energy security concerns. The use of wastes is particularly important because increased population growth is expected to create larger waste quantities that require appropriate management. For instance, in the developed world, approximately 1 waste tire per person per year is produced resulting in approximately 1 billion discarded tires annually [8]. In addition, there are currently an estimated 4 billion waste tires in landfills and stockpiles worldwide. In this paper, we study the use of waste tires because they are a particularly suitable feedstock for conversion to high-value products through gasification as a result of their homogeneous nature, high energy density (Lower Heating Value of ~ 33.96 MJ/kg, higher than coal), high volatile matter content ($\sim 67\%$) and low ash content ($\sim 7\%$) [9].

A further development to the polygeneration concept is to implement a flexible design which involves oversizing process equipment so as to allow adjustment of the production rates (and thus the product portfolio) in order to exploit market volatility. Thus, the flexible design problem involves optimizing the trade-offs between the increased capital costs associated with the larger equipment capacities and the expected increase in profit due to operational flexibility. This optimization problem can be formulated as a scenario-

based two-stage stochastic Mixed-Integer Nonlinear Program (MINLP) as explained in Section 2.1. The choice of equipment sizes is modeled using discrete first-stage variables (fixed before the realization of uncertainty) and the operating conditions are modeled using continuous second-stage variables (adjusted in response to realization of uncertainty). This optimization problem is typically nonconvex as a result of the nonlinear equations necessary to describe mixing, splitting and chemical reaction processes.

Such two-stage stochastic programs with recourse exhibit a special structure that makes them amenable to solution using duality-based decomposition approaches. For instance, the Benders decomposition (or L-shaped method) provides an efficient approach for solution of two-stage stochastic Mixed-Integer Linear Programs (MILPs) [10]. This strategy was extended to give the Generalized Benders Decomposition (GBD) algorithm that can solve two-stage stochastic Mixed-Integer Convex Programs (MICPs) [11]. However, nonconvex optimization problems generally do not satisfy strong duality, thus convergence cannot be guaranteed with GBD. This motivated Li et al. [12, 13] to develop the Nonconvex Generalized Benders Decomposition (NGBD) algorithm used in this paper which is summarized in Section 2.2. The NGBD algorithm is guaranteed to solve two-stage stochastic nonconvex MINLPs with discrete first-stage variables to global optimality. Furthermore, we use the GOSSIP software (recently developed by Kannan and Barton) that provides a versatile framework for modeling two-stage stochastic nonconvex MINLPs as well as their efficient solution using the NGBD algorithm [14].

Previous work on flexible polygeneration was done by Meerman et al. who studied the conversion of coal, biomass and oil residues to hydrogen, Fischer-Tropsch liquids, methanol, urea and electricity [15, 16]. The economic value of implementing various levels of flexibility was determined and an analysis on the favored feedstocks and products for each price scenario was presented. However, an optimization of the system design and operating conditions was not carried out. Farhat and Reichelstein presented a first-principles analysis on the economic performance of flexible polygeneration using a simplified case study of a coal to electricity and fertilizers process [17]. They derived a series of propositions to quantify the "value of flexible polygeneration" which could be subdivided into the "value of diversification" and "value of flexibility". While these propositions provide useful intuition, they only hold for flow sheets without interconnections (where the flow sheet could be represented as a tree) and no detailed process design or optimization was done. Chen et al. studied the optimal design and operation of a pro-

cess in which coal and biomass are co-gasified to produce a mix of naphtha, diesel, methanol or electricity [18]. The optimization problem was formulated first as a two-stage stochastic nonconvex Nonlinear Program (NLP) with a concave objective function and solved with BARON. In order to satisfy the requirement of having only discrete first-stage variables, the optimization problem was reformulated as an MINLP and solved using the NGBD algorithm enhanced with additional dual information [19]. Both feedstocks were converted in a single gasification unit, thus the option of generating multiple syngas streams followed by subsequent blending was not studied.

While the studies presented above highlight the value of implementing a flexible design for polygeneration processes, further research is necessary on the co-utilization of waste tires and natural gas. These feedstocks are converted into separate syngas streams of different qualities that can then be blended in appropriate ratios so as to exploit available synergies. Furthermore, this work studies the influence of the degree of market volatility on the expected profitability of the flexible polygeneration process. Thus, the objective of this paper is to study the optimal design and operation under uncertainty of such a hybrid feedstock flexible polygeneration system with a product portfolio consisting of electricity, methanol, dimethyl ether, olefins or liquefied (synthetic) natural gas.

This paper is organized as follows: Section 2 provides a brief overview of the two-stage stochastic programming approach for optimization under uncertainty, the GOSSIP software framework and the NGBD algorithm; Section 3 details the approach for process modeling and formulation of the optimization under uncertainty problem; Section 4 presents the results and a discussion of the computational performance of the NGBD algorithm versus the state-of-the-art ANTIGONE solver. We present our conclusions in Section 5.

2. Optimization under uncertainty

2.1. General structure of two-stage stochastic nonconvex MINLPs

Designing a flexible polygeneration process involves determining the optimal trade-offs between the increased capital costs as a result of over-sizing the process equipment and the increased net profit as a result of operational flexibility to exploit price peaks. In this work, we use the two-stage stochastic programming approach [20] to place these two trade-offs on a level basis. Two-stage stochastic programming divides the decision variables into two

categories: First-stage or design decision variables that are made before the realization of uncertainty and cannot be altered after plant construction and second-stage or operational variables that can be adjusted after the realization of uncertainty during the plant life time. Thus, first-stage variables correspond to the choice of equipment sizes while second-stage variables correspond to operating conditions (such as flow rates, split fractions etc.) for each scenario of uncertain parameters. A recent review of stochastic programming approaches for optimization of process systems under uncertainty is presented by Li and Grossmann [21].

In particular, the flexible design problem is formulated as a two-stage stochastic MINLP with a structure presented in Problem (SP), where $\mathbf{y}$ denotes the first-stage design decision variables; $\mathbf{x}_h$, p_h, $\boldsymbol{\omega}_h$ denote the second-stage operational decision variables, probability of occurrence and realization of the uncertain parameter vector in scenario h respectively; $\mathbf{c}$ denotes a vector corresponding to capital cost data and f_h is the objective function of the second-stage (recourse) problem indexed by scenario h (corresponding to the operating profit in that scenario); data matrix $\mathbf{A}$ and vector $\mathbf{b}$ define constraints on the first-stage variables; data matrix $\mathbf{B}$ and the functions $\mathbf{g}_h$ are used to represent scenario-dependent constraints; $\boldsymbol{Y}$ and $\boldsymbol{X}_h$ correspond to the bounds on $\mathbf{y}$ and $\mathbf{x}_h$ respectively. We note that the uncertain parameters are modeled using a random vector with finite support i.e., the vector of uncertainty parameters can take on one of a finite number of scenarios s, where $h \in \{1,...,s\}$ indexes the scenario set. Thus Problem (SP) corresponds to the deterministic equivalent problem.

$$
\begin{aligned}
\max_{\mathbf{y},\mathbf{x}_1,\ldots,\mathbf{x}_s} \quad & \mathbf{c}^{\mathrm{T}}\mathbf{y} + \sum_{h=1}^{s} p_h f_h(\mathbf{x}_h, \boldsymbol{\omega}_h) \\
\text{s.t.} \quad & \mathbf{A}\mathbf{y} \leq \mathbf{b}, \\
& \mathbf{B}\mathbf{y} + \mathbf{g}_h(\mathbf{x}_h, \boldsymbol{\omega}_h) \leq \mathbf{0}, \qquad \forall h \in \{1,...,s\}, \\
& \mathbf{y} \in \boldsymbol{Y}, \\
& \mathbf{x}_h \in \boldsymbol{X}_h, \qquad \forall h \in \{1,...,s\}
\end{aligned}
\tag{SP}
$$

We note that the flexible design problem (SP) satisfies the following assumptions (although the NGBD algorithm is more generally applicable [13]):

1. All first-stage variables are bounded and discrete and thus can be reformulated using binary variables and additional linear constraints i.e.,

$\mathbf{y} \in \{0,1\}^{n_y}$, where n_y denotes the number of first-stage variables. This requirement needs to be satisfied for guaranteed convergence of the NGBD algorithm.

2. All second-stage variables $\mathbf{x}_h$ are continuous.
3. All participating functions are assumed to be factorable (i.e., they can be expressed as a finite recursive composition of certain univariate and bivariate functions as detailed in [22])
4. All participating functions are assumed to be separable in the (first-stage) binary and (second-stage) continuous variables. In addition, the capital cost data are not subject to uncertainty and all participating functions are assumed to be affine in $\mathbf{y}$.

The objectives, process model and constraints of the flexible design problem are translated into the form of Problem (SP) as described in Section 3.

2.2. Overview of the NGBD algorithm and the GOSSIP software framework

Two-stage stochastic programs exhibit a special structure: The first-stage variables of Problem (SP) are complicating variables in the sense that fixing them allows the original optimization problem to be separated into a number of smaller independent subproblems. This suggests a solution approach that involves iterating between searching the space of first-stage variables followed by the space of second-stage variables. Geoffrion outlines a two-step conceptual framework for the synthesis of efficient mathematical programming algorithms based on this intuition: First, the original problem is manipulated (using techniques such as projection, dualization, inner linearization and outer linearization) to derive an equivalent "Master Problem" that is easier to solve, and second, solution strategies (such as piecewise, relaxation and restriction) are employed to reduce the master problem to a sequence of subproblems that ideally can be solved using efficient specialized solvers [23]. Duality-based decomposition approaches are an illustration of this strategy: For instance, the GBD algorithm can be viewed as a procedure of applying projection and dualization followed by relaxation and restriction [11, 24].

The NGBD algorithm is a generalization of the GBD algorithm to the class of problems containing participating functions that are nonconvex in the second-stage variables. The general principle is to iteratively solve a series of lower bounding and upper bounding problems until convergence to a globally optimal solution (within a specified tolerance). The lower bounding problem is formulated by convexifying the original problem (SP). The

current implementation employs the Auxiliary Variable Method detailed in [25] although alternative approaches based on McCormick relaxations [22] (or the differentiable variant [26]) could also be implemented. The GBD algorithm is used to solve the lower bounding problem. Once GBD converges with a solution to the lower bounding problem, an upper bounding problem is constructed by fixing the $\mathbf{y}$ variables to this lower bounding solution. This yields a nonconvex NLP that is also fully decomposable by scenario. Affine inequalities are added to the lower bounding problem to exclude previously visited solutions $\mathbf{y}$ and the procedure is iterated until convergence [27].

In order to provide a versatile framework for the formulation of two-stage stochastic nonconvex MINLPs and their efficient solution using the NGBD algorithm, the GOSSIP software was recently developed as detailed in [14]. A native C++-based modeling language is provided for the user to formulate an optimization problem which can be of the form of Problem (SP). Subroutines for parsing the user-defined model as well as pre-processing are implemented. In addition, subroutines for automatic construction of all the necessary subproblems for the NGBD algorithm as well as links to state-of-the-art optimization solvers for their solution are implemented. A link to ANTIGONE is also implemented to solve the deterministic equivalent problem without using a decomposition strategy [28].

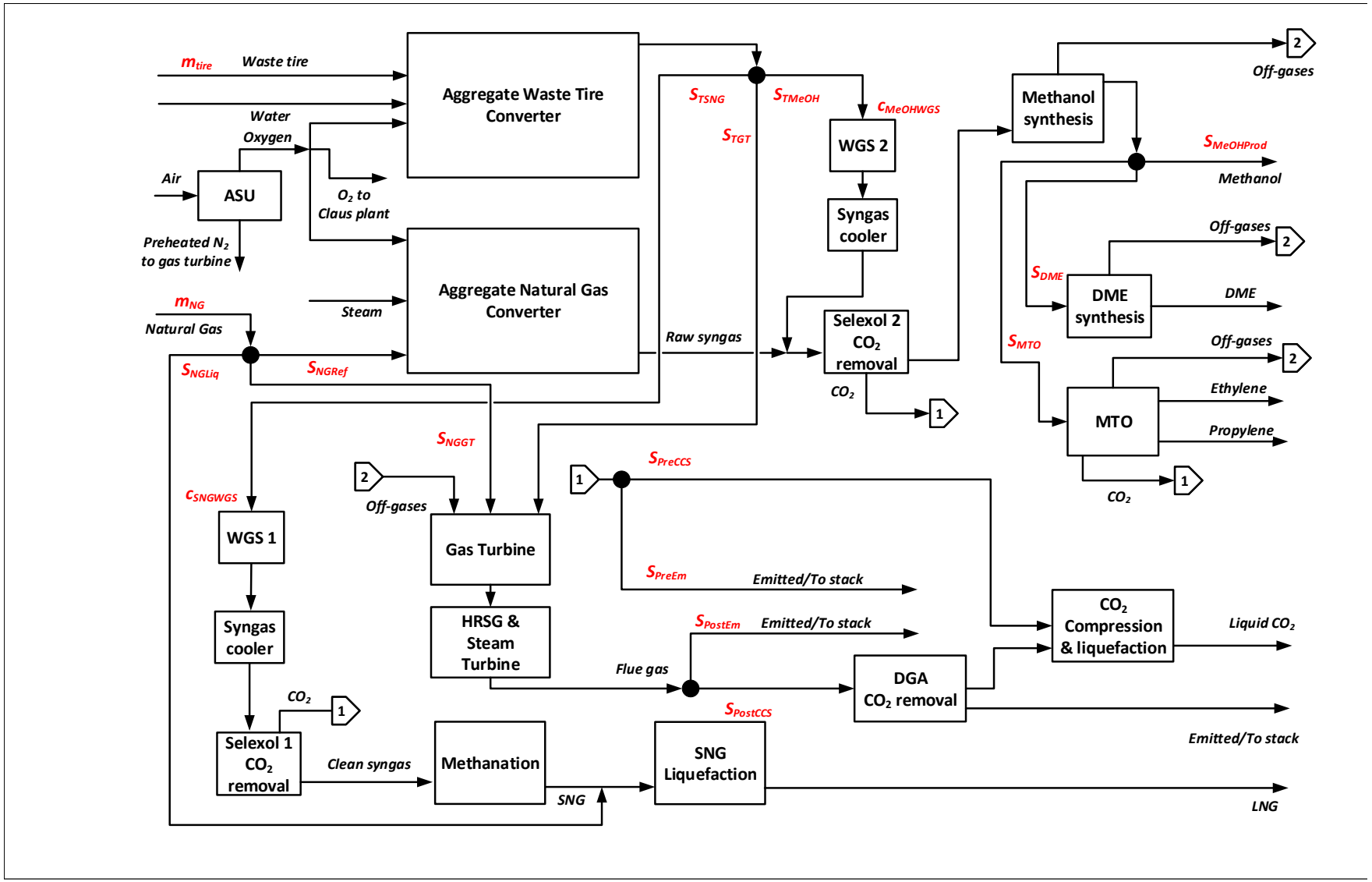

Figure 1: Superstructure of the hybrid natural gas and waste tire feedstock polygeneration system. The operational decision variables are indicated in red and presented in Table 2

Unit	Parameters	Reference
Tire Feedstock	Ultimate (wt%): C: 77.3, H: 6.2, N: 0.6, S: 1.8, O: 7.3, Ash: 6.8	[3]
	Proximate (wt%): VM: 67.7, FC: 25.5, Ash: 6.8	
Natural Gas (NG) Feedstock	T = 30 °C, P = 30 bar	[29]
	Composition (mol%): CH_4: 93.9, N_2: 0.008, CO_2: 0.01, C_2H_6: 0.032, C_3H_8: 0.007, C_4^+: 0.004	
Waste Tire Converter		
Waste tire preparation	Crumb size = 0.18 mm	[30]
Gasification	Entrained Flow gasification. 29.11 wt% water/70.88 wt% waste tire, P = 56 bar	[31]
	Oxygen to Tire ratio: 0.91, Ash melting energy: (1.0 kJ/kg_{ash})	[32]
COS hydrolysis	T = 200 °C, P = 54 bar	
H_2S removal	Solvent composition: 62.3 mol% DEPG: 37.7 mol% H_2O	[33]
	T = 40 °C, 53.5 bar, Removal: 92.7 % of H_2S	
Claus process	Two-stage sulfur conversion, Furnace: T = 950 °C	[34]
Natural Gas Converter		
NG pre-heater & pre-reformer	Pre-heater outlet T = 550 °C, Pre-reformer: T = 550 °C, P = 29.8 bar, Steam to NG ratio: 0.2	[1]
NG reformer	Autothermal reformer, Steam to NG ratio: 0.75, Oxygen to NG ratio: 0.95, Raw syngas cooled, dried & compressed to 55 bar	[1]
Air Separation Unit (ASU)	Oxygen purity: 99.5 mol%, Recovery pressure P = 10 bar	[6, 35]
Water Gas Shift (WGS)	High temperature WGS: T = 420 °C, P = 54 bar	[1, 6]
CO_2 removal	Solvent composition: 63.9 mol% DEPG: 36.1 mol% H_2O	[33]
	T = 20 °C, P = 53.5 bar, Removal: 96.9 % of CO_2	
Methanation	Four-stage conversion, Inlet T = 300 °C, Inlet P = 53.6 bar.	[36]
	Adiabatic reactors. Total ΔP = 3 bar (across 4 stages), Recycle ratio = 75 %	
SNG compression & purification	Outlet pressure = 55 bar	[34, 3]
SNG liquefaction	SNG flow rate = 9.7 kg/s, P = 55 bar, Inlet T = 22 °C, Outlet T = -157 °C	[29]
	MSHE UA_{max} = 25.0 MW/K, Pressure ratio = 6.5	
	Refrigerant mole composition: N_2: 8.3, CH_4: 24.0, C_2H_6: 36.9, n-C_4H_{10}: 30.8	
	Low P = 2.8 bar, high P = 18.0 bar, ΔT_{min} = 0.95 K, Flow rate = 58.5 kg/s	
Methanol synthesis & purification	T = 240 °C, P = 51 bar, Recycle ratio = 85 %, Off-gases to GT, Purity: 99.5 mol%	[37, 38]
DME synthesis & purification	T = 280 °C, P = 50 bar, Off-gases to GT	[38, 39]
	DME Purification column, Purity: 99.5 mol%	
MTO & purification	T = 400 °C, P = 40 bar, Off-gases to GT	[40]
	CO_2 absorption unit. Absorbent: 70.0 wt% DGA: 30.0 wt% H_2O, Absorber: 2 bar, Regenerator: 1.5 bar, Purity 99.9 mol%	
	De-ethanizer, 35 bar Ethane recovery: 99.80 %, Power consumption: 0.35 $MWe/MW_{LHV,Ethane}$	
	De-methanizer, 34 bar Methane removal: 99.99 % Power consumption: 1.21 $MWe/MW_{LHV,Methane}$	
	C2-splitter, 10 bar, Ethylene recovery: 95.00 %, purity: 99.9 mol%, Power consumption: 0.64 $MWe/MW_{LHV,Ethylene}$	
	De-propanizer, 25 bar, Propylene recovery: 98.00 %, purity: 99.2 mol%	
Gas Turbine	Thermal Efficiency: 46.8 % (Ratio of Net Power out [MW] to Total LHV of input fuel)	Simulation
Steam Turbine	Thermal Efficiency (High Quality heat): 44.1 %, Thermal Efficiency (Low Quality heat): 15.4 % (Details in Supp. Mat.)	[41, 42]
Postcombustion CO_2 capture	Solvent composition: 72.3 wt% DGA: 27.3 wt% H_2O	[33, 3]
	T = 70 °C, P = 1.0 bar, CO_2 Removal = 95.0 %	
CO_2 compression	Multistage compressors, CO_2 purity = 99.1 mol%, Outlet T = 25 °C, P = 153 bar	[35]
CO_2 transportation and sequestration	Operating cost: 12.5 $/tonne	[1]
Compressors	Isentropic efficiency = 80 %, maximum pressure ratio = 5	[1]
Pumps	Efficiency = 80 %	[1]

Table 1: Operating parameters and specifications used for the rigorous process simulation

3. Optimization Problem Formulation

3.1. Process Simulation and Surrogate Model

3.1.1. General description

Figure 1 presents a superstructure of the hybrid natural gas and solid waste tire feedstock polygeneration process that produces the following product portfolio: Electricity, liquefied (synthetic or well) natural gas, methanol, dimethyl ether, ethylene and propylene. Rigorous mass and energy balance models for the various sections of the superstructure are developed using either Aspen HYSYS v10 (for Selexol units) or Aspen Plus v10 (for all other units); an overview of the operating conditions used is presented in Table 1. A detailed presentation of the process modeling and simulation strategy is available in our previous work ([4] and [43]) where global optimization was performed without consideration of uncertainty. However, certain simplifications are made in the current work in order to keep the optimization problem computationally tractable when uncertainty is considered. An overview of the process model and changes made is presented next.

Operational decision variables for each scenario ($\mathbf{x}_h$) are presented in red in Figure 1 and described in Table 2. The total thermal input of the entire plant in each scenario h is determined by two (extensive) decision variables: The mass flow rates of waste tire ($m_{tire,h}$) and natural gas ($m_{NG,h}$). This plantwide thermal input is constrained to be less than 893 MW so as to provide a fair comparison with both our previous work ([3, 4, 43]) as well as a benchmark paper by Larson et al. [44]. All other operational decision variables are intensive.

3.1.2. Waste Tire train

In Figure 1, we define a nonstandard block termed "Aggregate Waste Tire Converter" that encompasses four sub-blocks. The first is a tire feedstock and slurry preparation unit in which rubber is separated out, ground into crumbs and mixed with water. The crumb tire slurry and oxygen from an air separation unit (ASU) are fed into the second sub-block consisting of an entrained flow gasifier (housed together with the radiant syngas cooling and quench system) that generates raw syngas. The third sub-block performs syngas cleaning and consists of a scrubber (for removal of particulates, sulfides and chlorides), COS hydrolysis (to H_2S) unit, syngas cooler and sour water knockout drum, a Selexol-based H_2S removal unit and a Claus unit (for conversion of captured H_2S to elemental sulfur). Slag flows down the

walls of the gasifier and falls down into the quench where it solidifies. The solids and ash are removed and treated in the fourth sub-block.

Compared to our previous work, two simplifications are made: The ratio of the oxygen to tire mass flow rate is fixed and the option for sulfur removal is implemented immediately after the gasifier. Since all other relevant operating conditions are fixed, these two simplifications imply that the surrogate mass balance model takes the form of a linear function (Equation 12) relating the clean syngas mole flow rate in scenario h ($f_{TDsweet\_gas,i,h}$) to $m_{tire,h}$. All the constants such as the mole fraction of component i belonging to the component set I ($x_{TDsweet\_gas,i}$), molecular weight ($MW_{TDsweet\_gas}$) and syngas yield (R_{ST} - the ratio of the mass flow rates of clean syngas to tire) of the clean syngas stream are determined directly from the Aspen Plus simulation. The H_2/CO mole ratio of the clean tire-derived syngas stream is ~ 0.7. We note that making the first simplification eliminates the need to implement a highly nonlinear (and thus nonconvex) surrogate model to represent the complex gasification process as was done in [43]; we found that performing optimization under uncertainty with such a model was computationally intractable even for a small number of scenarios because convexifying these constraints yields only weak lower bounds which in turn implies that the set of feasible candidate solutions of the first-stage binary variables does not shrink sufficiently quickly. An analogous argument holds for developing the surrogate energy balance model. Similarly, implementing the sulfur removal system immediately after the gasifier eliminates the (nonconvex) bilinear terms associated with an additional stream splitter. In addition, for the case of flexible polygeneration, we expect it to be cheaper to implement a single high-throughput sulfur removal system prior to the stream splitter that operates in a large number of scenarios than to implement multiple sulfur removal systems in the methanation and methanol synthesis trains (as done in [43]) that each operate in a smaller number of scenarios even though the latter option eliminates the need for a dedicated COS hydrolysis reactor.

$$f_{TDsweet\_gas,i,h} = \frac{x_{TDsweet\_gas,i} \cdot R_{ST} \cdot m_{tire,h}}{MW_{TDsweet\_gas}},\ \forall i \in I, \forall h \in \{1, ..., s\} \qquad (1)$$

The clean tire-derived syngas stream is then split into three branches heading to the methanation, gas turbine and methanol synthesis sections with the corresponding stream split fractions in scenario h denoted by $S_{TSNG,h}$, $S_{TGT,h}$ and $S_{TMeOH,h}$ respectively. The mass balance constraints are presented in Equation 14, where $f_{TMETH\_feed,i,h}$, $f_{TGT\_feed,i,h}$ and $f_{TMEOH\_feed,i,h}$ denote

the molar flow rates of component i in the tire-derived syngas stream heading to the methanation, gas turbine and methanol synthesis sections in scenario h respectively. We note that the bilinear terms in Equation 14 introduce nonconvexities; the reformulation-linearization technique (RLT) is used to generate a set of auxiliary mass balance constraints for the splitter that yield tighter convex relaxations for the lower bounding problem as presented in Section 3.1.6.

$$\begin{gathered} f_{TMETH\_feed,i,h} = f_{TDsweet\_gas,i,h} \cdot S_{TSNG,h},\ \forall i \in I, \forall h \in \{1, ..., s\} \\ f_{TGT\_feed,i,h} = f_{TDsweet\_gas,i,h} \cdot S_{TGT,h},\ \forall i \in I, \forall h \in \{1, ..., s\} \\ f_{TMEOH\_feed,i,h} = f_{TDsweet\_gas,i,h} \cdot S_{TMeOH,h},\ \forall i \in I, \forall h \in \{1, ..., s\} \\ S_{TSNG,h} + S_{TGT,h} + S_{TMeOH,h} = 1.0, \forall h \in \{1, ..., s\} \end{gathered} \tag{2}$$

3.1.3. Natural gas train

An analogous modeling approach is followed for the natural gas train: The natural gas feedstock is split into three streams that head to the liquefaction, gas turbine and methanol synthesis sections with the corresponding split fractions given by $S_{NGLiq,h}$, $S_{NGGT,h}$ and $S_{NGRef,h}$ respectively. Mass balance constraints of a similar form to Equation 14 together with auxiliary RLT constraints are implemented. For the natural gas stream heading to the methanol synthesis section, a block termed "Aggregate Natural Gas Converter" is defined that encompasses the natural gas pre-heater and pre-reformer, the reformer, scrubber and compressor for natural gas-derived syngas. Similar to the waste tire train, in this work we implement simpler linear surrogate mass and energy balance models for the natural gas conversion section by fixing the ratios of the converted natural gas stream and the steam and oxygen flow rates fed to the reformer. This yields a natural gas-derived syngas stream with a H_2/CO mole ratio of ~ 3.0.

3.1.4. Product synthesis trains

Tire-derived syngas heading to the methanation or methanol synthesis sections can be upgraded using a water gas shift (WGS) reactor; the overall conversion of CO in scenario h is an operational decision variable denoted by $c_{SNGWGS,h}$ and $c_{MeOHWGS,h}$ respectively. Prior to methanation, CO_2 is removed in a Selexol-based process. The H_2/CO mole ratio of the stream

heading to the first methanation reactor is constrained to be ~ 3.0. The produced synthetic natural gas stream is combined with the relevant natural gas branch prior to liquefaction to produce liquified natural gas (LNG). Conversely, in the methanol synthesis train, the natural gas-derived syngas stream is blended with the (upgraded) tire-derived syngas stream first before heading to the CO_2 removal and methanol synthesis sections. The H_2/CO mole ratio of the stream heading to the methanol synthesis reactor is constrained to be ~ 2.0. Thus this correct ratio can be attained either by using the appropriate tire and natural gas flow rates (and thereby exploiting synergies between the two feedstocks) or by employing the WGS reactor. For each scenario h, the produced methanol stream either heads to the DME synthesis section, the MTO section or is directly sold as the final product with the corresponding split fractions denoted by $S_{DME,h}$, $S_{MTO,h}$ and $S_{MeOHProd,h}$ respectively. This methanol splitter is modeled using a mass balance model similar to Equation 14 together with auxiliary RLT constraints. We note that with the exception of the stream splitter model, all other mass and energy balance constraints in the methanation and methanol synthesis trains are linear.

3.1.5. Power generation and CO_2 capture trains

For the gas turbine section, energy balance constraints are implemented by assuming a constant gas turbine efficiency such that the net work generated in each scenario is a linear function of the total thermal input (on a LHV basis) of the relevant natural gas and tire-derived syngas streams. A similar approach is used to determine the additional electricity generated in the steam turbine utilizing waste heat from the flue gas. The flue gas stream is either emitted or heads to a DGA-based postcombustion CO_2 capture unit with corresponding split fractions given by $S_{PostEm,h}$ or $S_{PostCCS,h}$ respectively. Similarly, the captured CO_2 streams from the Selexol units are either emitted or head to the CO_2 compression and liquefaction system with corresponding split fractions given by $S_{PreEm,h}$ and $S_{PreCCS,h}$ respectively. Both these splitters result in nonconvex mass balance constraints similar to Equation 14 in addition to RLT constraints.

3.1.6. Auxiliary Reformulation-Linearization Technique (RLT) constraints

The nonconvex bilinear terms introduced in Equation 14 potentially yield weak convex relaxations when constructing the lower bounding problem. This may result in slow convergence of the NGBD algorithm. Thus, it is

essential to augment the optimization model with relevant reformulation-linearization technique (RLT) constraints as detailed in [25] and [45]. These are a set of constraints that are redundant for the original Problem (SP) but are not redundant for its convex relaxation thereby yielding a tighter lower bounding problem. For the specific case of bilinear terms, the RLT constraints derived by Quesada and Grossmann are implemented which take the form of Equation 67 (corresponding to the constraints of Equation 14) [46]. Similar RLT constraints are implemented for the other equations involving bilinear terms. We note that Equation 67 has a physical interpretation as an alternative formulation of the splitter mass balance constraints although this is not always the case for other kinds of nonconvexities.

$$f_{TDsweet\_gas,i,h} = f_{TMETH\_feed,i,h} + f_{TGT\_feed,i,h} + f_{TMEOH\_feed,i,h}, \quad \forall i \in I, \forall h \in \{1, ..., s\} \tag{3}$$

3.2. Economic Model

3.2.1. Uncertainty Characterization

Table 3 presents the vector of uncertain parameters considered in this work which consists of the following components: The market prices of the six products, the waste tire tipping fees and the prevailing CO_2 tax rate. The uncertain parameter vector is assumed to be a random vector belonging to a normal distribution with the means and standard deviations listed in Table 3. The values for the means and standard deviations are determined from historical data obtained from the sources listed. The uncertain parameter vector ($\boldsymbol{\omega}_h$) is assumed to take on one of a finite number of scenarios s sampled from the normal distribution according to the approach presented by Li et al. [12]. Two different values of s are studied: 256 (2 scenarios for each of the 8 uncertain parameters) and 864 (3 scenarios for $P_{Elec,h}$, $P_{MeOH,h}$, $P_{Tire,h}$ and only 2 scenarios for the other uncertain parameters so as solve the problem in reasonable computation times). Furthermore, two cases are studied in this work. Case 1 investigates the optimization under uncertainty problem using the historical mean and standard deviation values presented in Table 3. However, in the interest of investigating the influence of higher volatility in market conditions, we also study an additional case (Case 2) in which the uncertain parameters have the same mean values as Case 1 but have higher standard deviations by 25%.

3.2.2. Expected Net Present Value (NPV) calculation

The objective of the optimization problem is to maximize the expected NPV of the flexible polygeneration plant as presented in Problem (FP). NPV is calculated using the Discounted Cash Flow Rate of Return approach with the assumptions made in [18] where R_{tax}, r, t_{dp} and t_{lf} denote the income tax rate, annual discount rate, depreciation time and project lifetime respectively.

Cap denotes the total capital cost. The polygeneration plant consists of 20 process sections (collected into a set U) and each section u can take on one size out of a discrete set of section sizes as presented in Equation 57, where $S_{u,j}$ is the j^{th} choice for size of the section, S_u^{LBD} and S_u^{UBD} are the lower and upper bounds on the section size, and d is the number of equipment sizes available (i.e., the cardinality of the discrete set of sizes) which is fixed to be 10 to keep the problem tractable.

$$S_{u,j} = S_u^{LBD} + \frac{j-1}{d-1} \cdot (S_u^{UBD} - S_u^{LBD}),\ \forall u \in U,\ \forall j \in \{1, ..., d\} \tag{4}$$

The capital cost associated with each section size $S_{u,j}$ (denoted $Cap_{u,j}$) is given by Equation 58, where $Cap_{u,0}$, $S_{u,0}$ and sf_u denote the base cost, base capacity and scaling factor of section u.

$$Cap_{u,j} = Cap_{u,0} \cdot \left(\frac{S_{u,j}}{S_{u,0}}\right)^{sf_u},\ \forall u \in U,\ \forall j \in \{1, ..., d\} \tag{5}$$

For each section u, the binary first-stage decision variables $y_{u,j}$ represents the choice of the j^{th} size, with $\mathbf{y}$ denoting a vector of these variables. Thus, the designed section size (S_u) and the corresponding capital cost (Cap_u) are presented in Equations 60 and 61 respectively, with Equation 59 representing the constraint that only one size can be chosen and Equation 62 giving the total capital costs (where K_L and K_{WC} are factors representing the additional costs associated with purchasing land and working capital).

$$S_u = \sum_{j=1}^{d} S_{u,j} \cdot y_{u,j},\ \forall u \in U \tag{6}$$

$$Cap_u = \sum_{j=1}^{d} Cap_{u,j} \cdot y_{u,j},\ \forall u \in U \tag{7}$$

$$\sum_{j=1}^{d} y_{u,j} = 1, \ \forall u \in U \tag{8}$$

$$Cap = (K_L + K_{WC}) \cdot \sum_{u \in U} Cap_u \tag{9}$$

The linking (complicating) constraints are presented in Equation 63, where the throughput for each section in scenario h ($F_{u,h}$) is constrained to be lower than the section's capacity.

$$F_{u,h} \leq S_u, \ \forall u \in U, \ \forall h \in \{1, ..., s\} \tag{10}$$

$Pro_{net,h}$ denotes the annual net profit in scenario h which is the difference between the annual revenues (from product sales and tipping fees) and the annual operating costs (consisting of variable operating costs such as feedstock costs, CO_2 taxes, utility, solvent, catalyst and waste disposal costs, and fixed operating costs including labor costs, operating overhead, property taxes and insurance). Details on the data and sources used for the economic model are presented in the Supplementary Material.

3.3. Summary of Optimization under Uncertainty Problem

Problem (FP) summarizes the flexible polygeneration problem which takes the form of a two-stage stochastic nonconvex MINLP. Problem (FP) has 200 binary first-stage decision variables, $435s$ continuous second-stage variables, 20 first-stage equality constraints, $412s$ second-stage equality constraints and $32s$ second-stage inequality constraints. We note that Problem (FP) has more than 100,000 variables and constraints (for $s = 256$) and close to 400,000 variables and constraints (for $s = 864$). The complete formulation of the optimization problem is presented in the Supplementary Material.

Operational decision variable ($\mathbf{x}_h$)	Description (for each scenario h $\in \{1, ..., s\}$)	Units	LBD	UBD
Waste tire train				
$m_{tire,h}$	Mass flow rate of waste tire	kg/s	0.0	26.3
$S_{TSNG,h}$	Split fraction of tire-derived syngas sent to methanation		0.0	1.0
$S_{TMeOH,h}$	Split fraction of tire-derived syngas sent to methanol synthesis		0.0	1.0
$S_{TGT,h}$	Split fraction of tire-derived syngas sent to the gas turbine		0.0	1.0
Natural gas train				
$m_{NG,h}$	Mass flow rate of natural gas	kg/s	0.0	18.7
$S_{NGRef,h}$	Split fraction of natural gas sent to reformer		0.0	1.0
$S_{NGGT,h}$	Split fraction of natural gas sent to gas turbine		0.0	1.0
$S_{NGLiq,h}$	Split fraction of natural gas sent for liquefaction		0.0	1.0
Downstream product trains				
$c_{SNGWGS,h}$	Overall conversion of CO in the WGS reactor prior to methanation		0.0	0.8
$c_{MeOHWGS,h}$	Overall conversion of CO in the WGS reactor prior to methanol synthesis		0.0	0.8
$S_{MeOHProd,h}$	Split fraction of methanol sold as product		0.0	1.0
$S_{DME,h}$	Split fraction of methanol sent to DME synthesis		0.0	1.0
$S_{MTO,h}$	Split fraction of methanol sent to MTO synthesis		0.0	1.0
CO_2 capture train				
$S_{PostCCS,h}$	Split fraction of flue gas sent to the DGA-based postcombustion CCS		0.0	1.0
$S_{PreCCS,h}$	Split fraction of CO_2 removed in other plant sections sent to sequestration		0.0	1.0
$S_{PostEm,h}$	Split fraction of flue gas sent to stack/emitted		0.0	1.0
$S_{PreEm,h}$	Split fraction of CO_2 removed in other plant sections sent to stack/emitted		0.0	1.0

Table 2: List of the 17 operating decision variables for the optimization problem

Uncertain parameter vector ($\boldsymbol{\omega}_h$)	Description	Units	Mean	Standard deviation	Source
$P_{NG,h}$ [1]	Natural gas price	\$/MMBtu	5.5	3.0	[47]
$P_{Elec,h}$	Hourly electricity price	\$/MWh	96.1	22.1	[48]
$P_{MeOH,h}$	Methanol price	\$/tonne	500	200	[49]
$P_{DME,h}$	DME price	\$/tonne	800	200	[50]
$P_{Ethylene,h}$	Ethylene price	\$/tonne	1050	360	[51]
$P_{Propylene,h}$	Propylene price	\$/tonne	1000	400	[52]
$P_{Tire,h}$	Waste tire tipping fee	\$/tonne	50	25	Assumed
$P_{CO_2,h}$	CO_2 tax rate	\$/tonne	50	25	Assumed

Table 3: Prices and CO_2 tax rate parameters for the scenarios. [1]A fixed premium of 65% is assumed for the price of LNG over the price of natural gas based on data from [47]

$$
\begin{aligned}
\max_{\mathbf{y},\mathbf{x}_1,\ldots,\mathbf{x}_s} \quad & \mathbb{E}_{\boldsymbol{\omega}}[\text{NPV}] = Cap(\mathbf{y}) \cdot \Big[-1 + \frac{R_{tax}}{r \cdot t_{dp}} \cdot \Big(1 - \frac{1}{(1+r)^{t_{dp}}}\Big)\Big] \\
& + \sum_{h=1}^{s} p_h \cdot Pro_{net,h}(\mathbf{x}_h, \boldsymbol{\omega}_h) \cdot \Big[\frac{1}{r} \cdot \Big(1 - \frac{1}{(1+r)^{t_{lf}}}\Big)\Big] \\
\text{s.t.} \quad & \text{First-stage constraints: Capital cost model,} \\
& \text{Second-stage constraints: Mass and energy balance model, } \forall h \in \{1,...,s\}, \\
& \qquad \text{Annual net profit model, Scale constraints, } \forall h \in \{1,...,s\}, \\
& \text{Linking constraints: Throughput}_h \leq \text{Equipment Capacity, } \forall h \in \{1,...,s\},
\end{aligned}
\tag{FP}
$$

4. Results and Discussion

4.1. Case 1: Using historical means and standard deviations

Table 4 presents the capital costs and expected operational characteristics of two proposed flexible polygeneration processes corresponding to the two characterizations of uncertainty studied (i.e., with 256 and 864 scenarios). For comparison, the results of the nominal design in which all uncertain parameters are assumed to take on their mean values are also presented. In the nominal (inflexible) design, methanol is favored as a primary product together with a small amount of electricity produced from combustion of off-gases and waste heat recovery. Both waste tire and natural gas are utilized as a feedstock with the syngas upgraded using a water gas shift reactor. We note that this outcome of production of only a single primary product by an inflexible design is consistent with previous empirical results [2, 4, 43, 18] as well as Proposition 1 of Farhat and Reichelstein [17].

In Flexible design 1, four products are produced in changing quantities over the plant life time: Liquified (S)NG, electricity, methanol and dimethyl ether. Thus, the operating conditions of the plant are adjusted in response to market conditions in order to produce the most profitable product portfolio at a given time. Higher capital investments are made at the design stage in order to provide this operational flexibility. In order to provide a fair comparison between the flexible and nominal design, the value of the stochastic solution (VSS as detailed in [20]) is calculated using Equation 11, where $\mathbb{E}_{\boldsymbol{\omega}}[\text{NPV}_{Flexible}]$ denotes the expected NPV of the flexible design and $\mathbb{E}_{\boldsymbol{\omega}}[\text{NPV}_{EVP}]$ denotes the expected NPV of the expected value problem (also

termed the expectation of the expected value problem). The expected value problem is formulated by fixing the first-stage design variables to those obtained with the nominal design; the stochastic program is then run with the same uncertainty characterization as the flexible design. Thus, the expectation of the expected value problem gives the NPV that would be obtained if the nominal design faces uncertainty belonging to the same distribution as that faced by the flexible design. Table 4 shows that implementing flexible designs gives a substantial VSS highlighting the importance of taking uncertainty into account.

$$\text{VSS} = \mathbb{E}_{\boldsymbol{\omega}}[\text{NPV}_{Flexible}] - \mathbb{E}_{\boldsymbol{\omega}}[\text{NPV}_{EVP}] \tag{11}$$

The expected product portfolio and operational characteristics are also presented which corresponds to the weighted average (by probability) over all scenarios of the values of the given operational variable. For each product, the terms in parenthesis denote the percentage of scenarios (weighted by probability) in which the product is produced. For instance, for Flexible design 1, this implies that electricity is produced in all scenarios, liquified (S)NG is produced in only 12.5 % of scenarios while methanol and DME are produced in half of all scenarios. We note that this implies that there exist certain scenarios in which liquified (S)NG is produced together with one of methanol or DME. Such a product portfolio may be attained in a scenario that primarily favors methanol (or DME) which is produced using most of the feedstock (by thermal input). However, given the discrete set of equipment sizes, a small amount of natural gas (corresponding to the difference between the maximum allowable thermal input and the thermal input used to produce methanol or DME) may head to the relatively cheap liquefaction section.

4.2. Case 2: Assuming 25 % higher standard deviations

Table 5 presents the corresponding results for the case with higher assumed variances (i.e., higher volatility) for all uncertain parameters. We note that the mean values of the uncertain parameters are unchanged thus the nominal design is identical to Case 1.

For Flexible design 1, the same design as in Case 1 is proposed but the plant attains a higher expected NPV. This can be explained as follows: For a scenario in which one product experiences an unusually high price, that product is favored. However, if that product experiences an unusually low price, operating conditions are adjusted to favor a different product in the

portfolio. For Flexible design 2, the solution favors implementing a larger aggregate waste tire converter to provide additional operational flexibility. This results in a higher expected production of electricity relative to Case 1. In Case 2, Flexible designs 1 and 2 result in a higher expected NPV compared to the corresponding flexible designs in Case 1. We note that this result of attaining a higher expected NPV with increasing price volatility (around the same mean) is consistent with Proposition 2a of Farhat and Reichelstein [17]. The VSS also increases compared to Case 1.

Case 1		Nominal design	Flexible design 1	Flexible design 2
Number of scenarios s		1	256	864
Capital costs				
Aggregate Waste Tire Converter	M$	198.2	198.2	198.2
Aggregate Natural Gas Converter	M$	60.0	60.0	60.0
Liquified (Synthetic) Natural Gas train				
Water Gas Shift 1	M$	0.0	0.0	0.0
CO_2 removal	M$	0.0	0.0	0.0
Methanation	M$	0.0	0.0	0.0
Liquefaction	M$	0.0	24.9	0.0
Methanol train				
Water Gas Shift 2	M$	9.7	9.7	9.7
CO_2 removal	M$	13.7	13.7	13.7
Methanol synthesis	M$	81.2	81.2	81.2
Dimethyl Ether (DME) synthesis	M$	0.0	100.5	100.5
Methanol-To-Olefins (MTO) process	M$	0.0	0.0	0.0
Power system [1]	M$	110.2	110.2	110.2
Post-combustion CO_2 capture	M$	0.0	0.0	0.0
CO_2 compression & sequestration	M$	4.6	4.6	4.6
Air Separation Unit	M$	164.6	164.6	164.6
Water systems	M$	63.2	77.4	77.4
Miscellaneous [2]	M$	52.6	52.6	52.6
Total capital costs (Cap)	M$	758.0	897.5	872.6
Expected product portfolio[3]				
Liquefied (S)NG	kg/s	0.0	1.4 (12.5 %)	0.0
Electricity	MW	14.2 (100 %) [4]	20.4 (100.0 %)	17.8 (100.0 %)
Methanol	kg/s	28.2 (100 %)	14.2 (50.0 %)	14.2 (50.0 %
Dimethyl Ether	kg/s	0.0	7.0 (50.0 %)	8.2 (50.0 %)
Ethylene	kg/s	0.0	0.0	0.0
Propylene	kg/s	0.0	0.0	0.0
Expected process operation				
Waste tire used	kg/s	10.0	9.2	9.1
Natural gas used	kg/s	11.6	12.1	11.8
Direct CO_2 emissions	kg/s	5.1	11.9	10.7
CO_2 sequestered	kg/s	13.8	6.2	7.3
Annual Net Profit	M$/year	155.4	231.8	214.4
Net Present Value (NPV)	M$	485.6	931.5	824.4
Expectation of expected value problem	M$	-	613.4	564.2
Value of the Stochastic Solution (VSS)	M$	-	318.1	260.2
Total wall time (NGBD)	s	155.2	3033.7	3219.6
Total wall time (ANTIGONE)	s	1.5	[5]	[5]

Table 4: Capital costs and expected operational characteristics of the two proposed flexible polygeneration processes compared with the nominal design for uncertainty characterized using historical means and standard deviations. [1] Includes the Gas Turbine, HRSG, Steam Turbine and Electricity accessory costs. [2] Miscellaneous includes Instrumentation & Control, Site preparation & improvement and Building & Structures. [3] The expected operational characteristic corresponds to the weighted average (by probability) over all scenarios of the values of the given operational variable. [4] The terms in parenthesis denote the percentage of scenarios (weighted by probability) in which the corresponding product is produced. [5] ANTIGONE was unable to provide a solution in 15,000 s.

Case 2		Nominal design [6]	Flexible design 1	Flexible design 2
Number of scenarios s		1	256	864
Capital costs				
Aggregate Waste Tire Converter	M$	198.2	198.2	322.0
Aggregate Natural Gas Converter	M$	60.0	60.0	60.0
Liquified (Synthetic) Natural Gas train				
Water Gas Shift 1	M$	0.0	0.0	0.0
CO_2 removal	M$	0.0	0.0	0.0
Methanation	M$	0.0	0.0	0.0
Liquefaction	M$	0.0	24.9	0.0
Methanol train				
Water Gas Shift 2	M$	9.7	9.7	9.7
CO_2 removal	M$	13.7	13.7	22.3
Methanol synthesis	M$	81.2	81.2	81.2
Dimethyl Ether (DME) synthesis	M$	0.0	100.5	100.5
Methanol-To-Olefins (MTO) process	M$	0.0	0.0	0.0
Power system [1]	M$	110.2	110.2	110.2
Post-combustion CO_2 capture	M$	0.0	0.0	0.0
CO_2 compression & sequestration	M$	4.6	4.6	5.8
Air Separation Unit	M$	164.6	164.6	164.6
Water systems	M$	63.2	77.4	77.4
Miscellaneous [2]	M$	52.6	52.6	52.6
Total capital costs (Cap)	M$	758.0	897.5	1006.2
Expected product portfolio[3]				
Liquefied (S)NG	kg/s	0.0	1.5 (12.5 %)	0.0
Electricity	MW	14.2 (100 %) [4]	20.8 (100 %)	22.6 (100 %)
Methanol	kg/s	28.2 (100 %)	14.2 (50.0 %)	13.3 (50.0 %
Dimethyl Ether	kg/s	0.0	6.9 (50.0 %)	7.9 (50.0 %)
Ethylene	kg/s	0.0	0.0	0.0
Propylene	kg/s	0.0	0.0	0.0
Expected process operation				
Waste tire used	kg/s	10.0	9.1	14.0
Natural gas used	kg/s	11.6	12.2	8.5
Direct CO_2 emissions	kg/s	5.1	11.9	15.0
CO_2 sequestered	kg/s	13.8	6.0	9.4
Annual Net Profit	M$/year	155.4	254.9	248.3
Net Present Value (NPV)	M$	485.6	1,104.6	958.2
Expectation of expected value problem	M$	-	699.7	627.3
Value of the Stochastic Solution (VSS)	M$	-	404.9	330.9
Total wall time (NGBD)	s	155.2	2277.2	2955.4
Total wall time (ANTIGONE)	s	1.5	[5]	[5]

Table 5: Capital costs and expected operational characteristics of the two proposed flexible polygeneration processes compared with the nominal design for uncertainty characterized using historical means but with standard deviations assumed to be 25 % higher than average. [1] Includes the Gas Turbine, HRSG, Steam Turbine and Electricity accessory costs. [2] Miscellaneous includes Instrumentation & Control, Site preparation & improvement and Building & Structures. [3] The expected operational characteristics correspond to the weighted average (by probability) over all scenarios of the values of the given operational variable. [4] The terms in parenthesis denote the percentage of scenarios (weighted by probability) in which the corresponding product is produced. [5] ANTIGONE was unable to provide a solution in 15,000 s. [6] The nominal design is identical to that of Case 1.

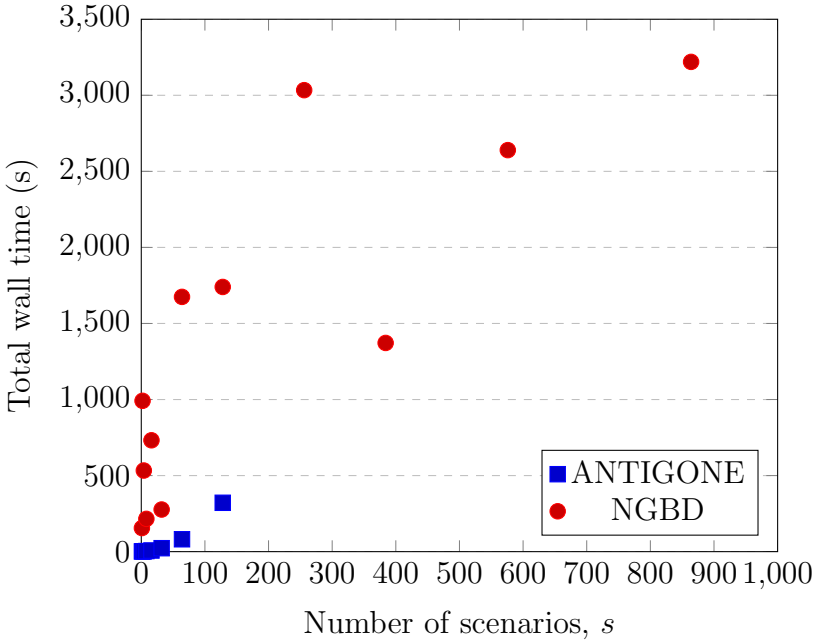

Figure 2: Scaling of solution times of NGBD and ANTIGONE with the number of scenarios

4.3. Computational Performance

Figure 2 presents the scaling of solution times of NGBD and ANTIGONE with number of scenarios. The procedure to generate these scenarios is presented in the Supplementary Material. When more than 128 scenarios are considered, ANTIGONE is unable to locate the global optimum within 15,000 s. Thus, NGBD scales favorably compared to ANTIGONE as the optimization under uncertainty problem becomes larger. However, NGBD performs worse than ANTIGONE for a smaller number of scenarios as the set of feasible candidate solutions of the first-stage binary variables does not shrink sufficiently quickly. We note that implementing RLT constraints was essential for convergence of NGBD in reasonable time.

5. Conclusions

The optimal design and operation under uncertainty of a hybrid feedstock flexible polygeneration system with a product portfolio consisting of electricity, methanol, dimethyl ether, olefins or liquefied (synthetic) natural gas is studied. The optimization problem is formulated as a recourse-based

two-stage stochastic nonconvex MINLP with first-stage variables corresponding to design decisions and second-stage variables to operational decisions. The recently developed GOSSIP software framework is used to model and efficiently solve the resulting formulations using the NGBD algorithm.

Two different characterizations of uncertainty are studied: In the first case study, the uncertain parameters are assumed to belong to independent normal distributions with means and standard deviations estimated using historical data. In the second case study, the standard deviations of the uncertain parameters are increased by 25 % in order to evaluate the impact of higher volatility. For each of these two cases, two flexible designs are developed based on a different number of scenarios. Implementing flexible designs is shown to result in an increase of expected net present value (compared to a nominal inflexible design) as well as a value of the stochastic solution in the range of 260 - 405 M$ for a scale of approximately 893 MW of thermal energy input. Price volatility around the same mean is shown to result in higher expected net present value and value of the stochastic solution as operational flexibility allows for asymmetric exploitation of price peaks.

Acknowledgements

A.S. gratefully acknowledges the financial support from NTNU's Department of Energy and Process Engineering and from NTNU Energy. R.K. gratefully acknowledges the support of the U.S. Department of Energy through the LANL/LDRD Program and the Center for Nonlinear Studies. This publication has been funded by HighEFF - Centre for an Energy-Efficient and Competitive Industry for the Future. The authors gratefully acknowledge the financial support from the Research Council of Norway and user partners of HighEFF, an 8-years Research Centre under the FME-scheme (Centre for Environment-friendly Energy Research, 257632).

Conflicts of Interest

The authors declare no conflicts of interest.

References

[1] T. A. Adams II, P. I. Barton, Combining coal gasification and natural gas reforming for efficient polygeneration, Fuel Processing Technology 92 (2011) 639–655.

[2] T. A. Adams II, J. H. Ghouse, Polygeneration of fuels and chemicals, Current Opinion in Chemical Engineering 10 (2015) 87–93.

[3] A. S. R. Subramanian, T. Gundersen, T. A. Adams II, Technoeconomic analysis of a waste tire to liquefied synthetic natural gas (SNG) energy system, Energy (2020) 117830.

[4] A. S. R. Subramanian, T. Gundersen, T. A. Adams II, Optimal design and operation of a waste tire feedstock polygeneration system, Energy (2021) 11990.

[5] A. M. Niziolek, O. Onel, M. F. Hasan, C. A. Floudas, Municipal solid waste to liquid transportation fuels–Part II: Process synthesis and global optimization strategies, Computers & Chemical Engineering 74 (2015) 184–203.

[6] I. J. Okeke, T. A. Adams II, Combining petroleum coke and natural gas for efficient liquid fuels production, Energy 163 (2018) 426–442.

[7] Y. K. Salkuyeh, T. A. Adams II, Integrated petroleum coke and natural gas polygeneration process with zero carbon emissions, Energy 91 (2015) 479–490.

[8] J. D. Martınez, N. Puy, R. Murillo, T. Garcıa, M. V. Navarro, A. M. Mastral, Waste tyre pyrolysis: A review, Renewable and Sustainable Energy Reviews 23 (2013) 179–213.

[9] V. Belgiorno, G. De Feo, C. Della Rocca, R. Napoli, Energy from gasification of solid wastes, Waste management 23 (2003) 1–15.

[10] J. F. Benders, Partitioning procedures for solving mixed-variables programming problems, Numerische mathematik 4 (1962) 238–252.

[11] A. M. Geoffrion, Generalized Benders decomposition, Journal of Optimization Theory and Applications 10 (1972) 237–260.

[12] X. Li, A. Tomasgard, P. I. Barton, Nonconvex Generalized Benders Decomposition for stochastic separable mixed-integer nonlinear programs, Journal of Optimization Theory and Applications 151 (2011) 425.

[13] X. Li, A. Sundaramoorthy, P. I. Barton, Nonconvex Generalized Benders Decomposition, in: Optimization in Science and Engineering, Springer, 2014, pp. 307–331.

[14] R. Kannan, Algorithms, analysis and software for the global optimization of two-stage stochastic programs, Ph.D. thesis, Massachusetts Institute of Technology, 2017.

[15] J. Meerman, A. Ramırez, W. Turkenburg, A. Faaij, Performance of simulated flexible integrated gasification polygeneration facilities. Part A: A technical-energetic assessment, Renewable and Sustainable Energy Reviews 15 (2011) 2563–2587.

[16] J. Meerman, A. Ramırez, W. Turkenburg, A. Faaij, Performance of simulated flexible integrated gasification polygeneration facilities, Part B: Economic evaluation, Renewable and Sustainable Energy Reviews 16 (2012) 6083–6102.

[17] K. Farhat, S. Reichelstein, Economic value of flexible hydrogen-based polygeneration energy systems, Applied Energy 164 (2016) 857–870.

[18] Y. Chen, T. A. Adams II, P. I. Barton, Optimal design and operation of flexible energy polygeneration systems, Industrial & Engineering Chemistry Research 50 (2011) 4553–4566.

[19] Y. Chen, X. Li, T. A. Adams II, P. I. Barton, Decomposition strategy for the global optimization of flexible energy polygeneration systems, AIChE Journal 58 (2012) 3080–3095.

[20] J. R. Birge, F. Louveaux, Introduction to stochastic programming, Springer Science & Business Media, 2011.

[21] C. Li, I. E. Grossmann, A Review of Stochastic Programming Methods for Optimization of Process Systems under Uncertainty, Frontiers in Chemical Engineering 2 (2020) 34.

[22] A. Mitsos, B. Chachuat, P. I. Barton, McCormick-based relaxations of algorithms, SIAM Journal on Optimization 20 (2009) 573–601.

[23] A. M. Geoffrion, Elements of large-scale mathematical programming Part I: Concepts, Management Science 16 (1970) 652–675.

[24] A. M. Geoffrion, Elements of large scale mathematical programming part II: Synthesis of algorithms and bibliography, Management Science 16 (1970) 676–691.

[25] M. Tawarmalani, N. V. Sahinidis, Convexification and global optimization in continuous and mixed-integer nonlinear programming: theory, algorithms, software, and applications, volume 65, Springer Science & Business Media, 2013.

[26] K. A. Khan, H. A. Watson, P. I. Barton, Differentiable McCormick relaxations, Journal of Global Optimization 67 (2017) 687–729.

[27] E. Balas, R. Jeroslow, Canonical cuts on the unit hypercube, SIAM Journal on Applied Mathematics 23 (1972) 61–69.

[28] R. Misener, C. A. Floudas, ANTIGONE: Algorithms for Continuous/Integer Global Optimization of Nonlinear Equations, Journal of Global Optimization 59 (2014) 503–526.

[29] H. A. Watson, M. Vikse, T. Gundersen, P. I. Barton, Optimization of single mixed-refrigerant natural gas liquefaction processes described by nondifferentiable models, Energy 150 (2018) 860–876.

[30] N. Sunthonpagasit, M. R. Duffey, Scrap tires to crumb rubber: feasibility analysis for processing facilities, Resources, Conservation and recycling 40 (2004) 281–299.

[31] M. C. Woods, P. Capicotto, J. L. Haslbeck, N. J. Kuehn, M. Matuszewski, L. L. Pinkerton, M. D. Rutkowski, R. L. Schoff, V. Vaysman, Cost and performance baseline for fossil energy plants, National Energy Technology Laboratory (2007).

[32] C. Kunze, H. Spliethoff, Modelling, comparison and operation experiences of entrained flow gasifier, Energy Conversion and Management 52 (2011) 2135–2141.

[33] T. A. Adams II, Y. K. Salkuyeh, J. Nease, Processes and simulations for solvent-based CO2 capture and syngas cleanup, in: Reactor and process design in sustainable energy technology, Elsevier, 2014, pp. 163–231.

[34] R. Brasington, J. Haslbeck, N. Kuehn, E. Lewis, L. Pinkerton, M. Turner, E. Varghese, M. Woods, Cost and Performance Baseline for Fossil Energy Plants — Volume 2: Coal to Synthetic Natural Gas and Ammonia, Technical Report, DOE/NETL-2010/1402, 2011.

[35] J. Klara, M. Woods, P. Capicotto, J. Haslbeck, N. Kuehn, M. Matuszewski, L. Pinkerton, M. Rutkowski, R. Schoff, V. Vaysman, Cost and performance baseline for fossil energy plants volume 1: Bituminous coal and natural gas to electricity. National Energy Technology Laboratory, Research and Development Solutions, LLC (RDS) (2007).

[36] N. Kezibri, C. Bouallou, Conceptual design and modelling of an industrial scale power to gas-oxy-combustion power plant, International Journal of Hydrogen Energy 42 (2017) 19411–19419.

[37] Y. Su, L. Lü, W. Shen, et al., An efficient technique for improving methanol yield using dual CO 2 feeds and dry methane reforming, Frontiers of Chemical Science and Engineering (2019) 1–15.

[38] Y. K. Salkuyeh, T. A. Adams II, A new power, methanol, and DME polygeneration process using integrated chemical looping systems, Energy conversion and management 88 (2014) 411–425.

[39] J. A. Scott, T. A. Adams II, Biomass-gas-and-nuclear-to-liquids (BGNTL) processes. Part I: Model development and simulation, The Canadian Journal of Chemical Engineering 96 (2018) 1853–1871.

[40] Y. Salkuyeh, T. A. Adams II, Co-production of olefins, fuels, and electricity from conventional pipeline gas and shale gas with near-zero CO2 emissions. Part I: process development and technical performance, Energies 8 (2015) 3739–3761.

[41] Y. Chen, Optimal design and operation of energy polygeneration systems, Ph.D. thesis, Massachusetts Institute of Technology, 2013.

[42] Y. Chen, T. A. Adams II, P. I. Barton, Optimal design and operation of static energy polygeneration systems, Industrial & Engineering Chemistry Research 50 (2010) 5099–5113.

[43] A. S. Subramanian, T. Gundersen, P. I. Barton, T. A. Adams II, Global optimization of a hybrid waste tire and natural gas feedstock polygeneration system, Energy (2022) 123722.

[44] E. D. Larson, H. Jin, F. E. Celik, Large-scale gasification-based coproduction of fuels and electricity from switchgrass, Biofuels, Bioproducts and Biorefining 3 (2009) 174–194.

[45] R. Misener, C. A. Floudas, GloMIQO: Global mixed-integer quadratic optimizer, Journal of Global Optimization 57 (2013) 3–50.

[46] I. Quesada, I. E. Grossmann, Global optimization of bilinear process networks with multicomponent flows, Computers & Chemical Engineering 19 (1995) 1219–1242.

[47] U.S. Energy Information Administration. Natural Gas Prices., https://www.eia.gov/dnav/ng/ng_pri_sum_dcu_nus_m.htm, 2020. [Online; accessed 11-June-2020].

[48] Ontario Independent Electricity System Operator (IESO). Hourly Ontario Energy Price, http://www.ieso.ca/en/Power-Data/Price-Overview/Hourly-Ontario-Energy-Price, 2020. [Online; accessed 11-June-2020].

[49] Methanex Monthly Average Regional Posted Contract Price History, https://www.methanex.com/our-business/pricing, 2020. [Online; accessed 11-June-2020].

[50] Alibaba. Dimethyl Ether Prices., https://www.alibaba.com/product-detail/Competitive-dimethyl-ether-prices_60506781674.html?spm=a2700.galleryofferlist.0.0.29d77a22XwD6XM, 2020. [Online; accessed 11-June-2020].

[51] Independent Commodity Intelligence Services. Ethylene US prices., https://www.icis.com/explore/commodities/chemicals/ethylene/us/, 2020. [Online; accessed 11-June-2020].

[52] Independent Commodity Intelligence Services. Propylene US prices., https://www.icis.com/explore/commodities/chemicals/propylene/us/, 2020. [Online; accessed 11-June-2020].

[53] M. Tawarmalani, N. V. Sahinidis, A polyhedral branch-and-cut approach to global optimization, Mathematical programming 103 (2005) 225–249.

[54] P. Belotti, J. Lee, L. Liberti, F. Margot, A. Wächter, Branching and bounds tighteningtechniques for non-convex MINLP, Optimization Methods & Software 24 (2009) 597–634.

[55] T. Achterberg, SCIP: solving constraint integer programs, Mathematical Programming Computation 1 (2009) 1–41.

[56] R. M. Van Slyke, R. Wets, L-shaped linear programs with applications to optimal control and stochastic programming, SIAM Journal on Applied Mathematics 17 (1969) 638–663.

[57] S. Boyd, L. Vandenberghe, Convex optimization, Cambridge university press, 2004.

[58] D. P. Bertsekas, Nonlinear Programming, Athena Scientific, 1999.

[59] J. Jensen, J. Poulsen, N. Andersen, From coal to clean energy, Nitrogen+ syngas 310 (2011) 34–38.

[60] Z. Y. Yeo, T. L. Chew, P. W. Zhu, A. R. Mohamed, S.-P. Chai, Conventional processes and membrane technology for carbon dioxide removal from natural gas: A review, Journal of Natural Gas Chemistry 21 (2012) 282–298.

[61] K. V. Bussche, G. Froment, A steady-state kinetic model for methanol synthesis and the water gas shift reaction on a commercial Cu/ZnO/Al2O3catalyst, Journal of Catalysis 161 (1996) 1–10.

[62] G. Bercic, J. Levec, Catalytic Dehydration of Methanol to Dimethyl Ether. Kinetic Investigation and Reactor Simulation, Industrial & engineering chemistry research 32 (1993) 2478–2484.

[63] L. Rath, Cost and performance baseline for fossil energy plants volume 2: coal to synthetic natural gas and ammonia. National Energy Technology Laboratory, DoE/NETL, report 1402 (2011).

[64] M. J. Tijmensen, A. P. Faaij, C. N. Hamelinck, M. R. van Hardeveld, Exploration of the possibilities for production of fischer tropsch liquids and power via biomass gasification, Biomass and Bioenergy 23 (2002) 129–152.

[65] C. N. Hamelinck, A. P. Faaij, H. den Uil, H. Boerrigter, Production of FT transportation fuels from biomass; technical options, process analysis and optimisation, and development potential, Energy 29 (2004) 1743–1771.

[66] S. Bashadi, H. Herzog, Using Aspen Icarus to simulate CO2 capture economics of IGCC Selexol process, in: BP-MIT Advanced Conversion Research Conference, Cambridge, MA.

[67] E. D. Larson, R. Tingjin, Synthetic fuel production by indirect coal liquefaction, Energy for sustainable Development 7 (2003) 79–102.

[68] E. D. Larson, H. Jin, F. E. Celik, Gasification-based fuels and electricity production from biomass, without and with carbon capture and storage, Princeton Environmental Institute, Princeton University (2005).

[69] D. Xiang, S. Yang, X. Liu, Z. Mai, Y. Qian, Techno-economic performance of the coal-to-olefins process with CCS, Chemical Engineering Journal 240 (2014) 45–54.

[70] L. Van Bibber, E. Shuster, M. Haslbeck, J.and Rutkowski, S. Olson, S. Kramer, Baseline Technical and Economic Assessment of a Commercial Scale Fischer-Tropsch Liquids Facility, DOE/NETL-2007-1260 (2007).

[71] P. Worhack, J. Haslbeck, Recommended Project Finance Structures for the Economic Analysis of Fossil-Based Energy Projects, DOE/NETL-401/090808 (2008).

[72] W. D. Seider, J. D. Seader, D. R. Lewin, Product & Process Design Principles: Synthesis, Analysis and Evaluation, John Wiley & Sons, 2009.

Supplementary Material 1: Benders Decomposition Algorithm for Two-Stage Stochastic Programming

This section provides an intuitive explanation of the Nonconvex Generalized Benders Decomposition Algorithm.

The size of Problem SP increases with the total number of scenarios considered. State-of-the-art solvers for nonconvex MINLPs such as BARON [53], ANTIGONE [28], COUENNE [54] and SCIP [55] implement algorithms for which the solution time increases exponentially with problem size. Thus, solving Problem SP with these general-purpose solvers quickly becomes computationally intractable as the number of scenarios is increased. However, Problem SP is not a general nonconvex MINLP but instead possesses a special structure that can be exploited to develop more efficient solution algorithms. First, we illustrate this special structure visually for the subclass of two-stage stochastic MILPs (presented in Problem SMILP-DEP) and then describe it for the two-stage stochastic MINLP of Problem SP. The data vectors $\mathbf{d}_h$ and $\mathbf{e}_h$, and matrix $_h$ depend on the realization of the uncertain parameter in scenario h.

$$
\begin{aligned}
\min_{\mathbf{y},\mathbf{x}_1,\ldots,\mathbf{x}_s} \quad & \mathbf{c}^{\mathrm{T}}\mathbf{y} + \sum_{h=1}^{s} p_h {\mathbf{d}_h}^{\mathrm{T}}\mathbf{x}_h \\
\text{s.t.} \quad & \mathbf{A}\mathbf{y} \leq \mathbf{b}, \\
& \mathbf{B}_h\mathbf{y} +_h \mathbf{x}_h \leq \mathbf{e}_h, \qquad \forall h \in \{1,\ldots,s\}, \\
& \mathbf{y} \in \boldsymbol{Y}, \\
& \mathbf{x}_h \in \boldsymbol{X}_h, \qquad \forall h \in \{1,\ldots,s\}
\end{aligned}
\tag{SMILP-DEP}
$$

In particular, we illustrate the structure of the constraints

$$\mathbf{B}_h\mathbf{y} +_h \mathbf{x}_h \leq \mathbf{e}_h, \forall h \in \{1,\ldots,s\}$$

with Figure 3.
We observe the following:

- Problem SMILP-DEP has an "almost block-diagonal" structure in the sense that if the vector of variables $\mathbf{y}$ is fixed (i.e., the blue portions of Figure 3 are fixed), then it becomes fully decomposable into a set of linear programming (LP) problems (one for each $h \in \{1,\ldots,s\}$) . In

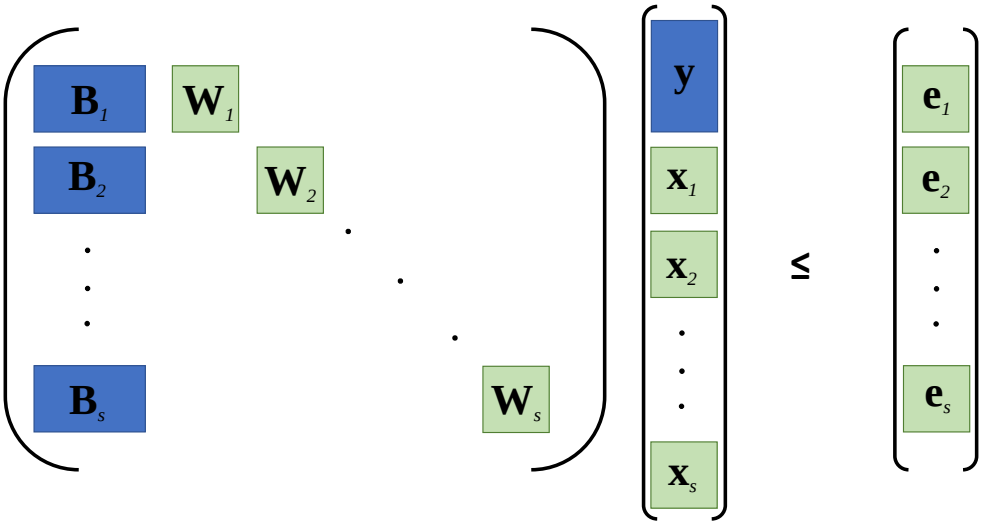

Figure 3: Illustration of special structure of two-stage stochastic MILPs

other words, to partition Problem SMILP-DEP, we begin by writing out an equivalent optimization problem (Problem SMILP-PART which only searches the space of the first-stage $\mathbf{y}$ variables). The objective function of Problem SMILP-PART is defined implicitly in terms of the solutions to the embedded Problems $\text{LP}_h(\mathbf{y})$ for all $h \in \{1, \ldots, s\}$.

- The set $\boldsymbol{V}$ contains all the feasible values of $\mathbf{y}$ for which all the embedded Problems $\text{LP}_h(\mathbf{y})$ have at least one feasible point. We note that constructing the set $\boldsymbol{V}$ algorithmically is challenging as it would require testing all the Problems $\text{LP}_h(\mathbf{y})$ for feasibility for each candidate member $\mathbf{y}$. This challenge is addressed in Section 5 where a duality theory-based reformulation is used to derive an equivalent set of "Benders Feasibility cuts" that characterizes set $\boldsymbol{V}$.

- Problems $\text{LP}_h(\mathbf{y})$ are parameterized by the particular value of the complicating variables $\mathbf{y}$. Thus, the Problems $\text{LP}_h(\mathbf{y})$ are constructed with $\mathbf{y}$ appearing on the right-hand side of the constraints (i.e., $\mathbf{y}$ is not a decision variable of Problems $\text{LP}_h(\mathbf{y})$).

- The key point is that the size of each of the Problems $\mathrm{LP}_h(\mathbf{y})$ is independent of the number of scenarios. In addition, the problem size is smaller allowing for more efficient solution.
- Problems SMILP-DEP and SMILP-PART have the same optimal objective function value.
- The problems $\mathrm{LP}_h(\mathbf{y})$ can be solved in parallel using a multi-core architecture (although this is not implemented in this work).

$$\begin{aligned} \min_{\mathbf{y}} \quad & \mathbf{c}^{\mathrm{T}}\mathbf{y} + \sum_{h=1}^{s} v_h(\mathbf{y}) \\ \text{s.t.} \quad & \mathbf{y} \in \boldsymbol{V} \equiv \left\{ \mathbf{y} \in \boldsymbol{Y} : \mathbf{A}\mathbf{y} \leq \mathbf{b} \text{ and } \exists \mathbf{x}_h \in \boldsymbol{X}_h :_h \mathbf{x}_h \leq \mathbf{e}_h - \mathbf{B}_h\mathbf{y}, \forall h \in \{1,\ldots,s\} \right\} \subset \boldsymbol{Y} \end{aligned} \tag{SMILP-PART}$$

$$\begin{aligned} v_h(\mathbf{y}) \quad = \quad & \min_{\mathbf{x}_h} \quad p_h {\mathbf{d}_h}^{\mathrm{T}} \mathbf{x}_h \\ & \text{s.t.} \quad {}_h\mathbf{x}_h \leq \mathbf{e}_h - \mathbf{B}_h\mathbf{y}, \\ & \qquad \mathbf{x}_h \in \boldsymbol{X}_h, \end{aligned} \tag{$\mathrm{LP}_h(\mathbf{y})$}$$

This strategy of fixing the complicating first-stage $\mathbf{y}$ variables to particular values and then decomposing the problem into a number of smaller independent subproblems can also be applied to Problem SP. The solution strategy involves iterating between searching the space of first-stage $\mathbf{y}$ variables followed by the space of second-stage $\mathbf{x}_h$ variables.

This intuition is used to derive efficient mathematical programming algorithms for two-stage stochastic programs:

- The earliest algorithm termed Benders Decomposition (BD) [10] or the L-shaped method [56] is applicable to two-stage stochastic LPs or MILPs.
- Next, the Generalized Benders Decomposition algorithm (GBD) [11] was developed and is applicable to two-stage stochastic MICPs.
- Recently. the Nonconvex Generalized Benders Decomposition algorithm (NGBD) [12, 13] was developed and is applicable to two-stage stochastic nonconvex MINLPs.

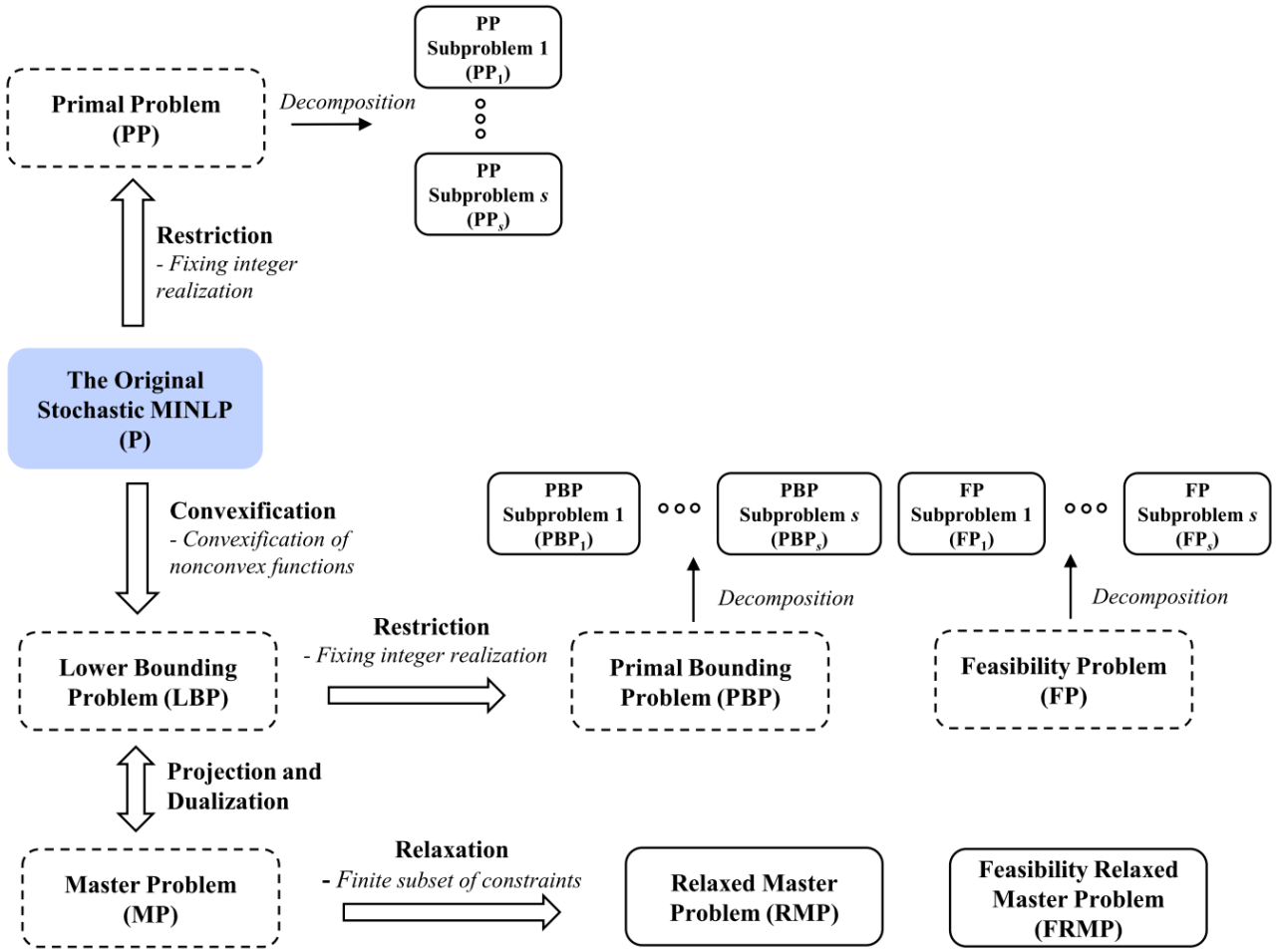

Figure 4: Overview of the Nonconvex Generalized Benders Decomposition (NGBD) algorithm. Reprinted from [12] with permission from Springer Nature. Only (sub)problems with solid outlines are solved.

Nonconvex Generalized Benders Decomposition (NGBD)

This section presents the NGBD algorithm which reduces to the GBD or BD algorithms for the corresponding problem classes. Emphasis is on describing the key concepts intuitively with a more rigorous presentation available in [12, 13, 14]. An overview of the NGBD algorithm is presented in Figure 4. The general principle is to iteratively solve a series of lower bounding and upper bounding problems until convergence to a globally optimum solution (within a specified tolerance).

The Lower Bounding Problem (LBP)

Problem SP is convexified using the Auxiliary Variables and Constraints Method to give Problem LBP where f_h^{cv} and $\mathbf{g}_h^{cv}$ are convex functions. Thus, Problem LBP is usually of a higher dimension than Problem SP since additional variables $\mathbf{q}_h$ are introduced together with corresponding constraints.

$$\begin{aligned}
\min_{\mathbf{y},\mathbf{x}_1,\ldots,\mathbf{x}_s,\mathbf{q}_1,\ldots,\mathbf{q}_s} \quad & \mathbf{c}^{\mathrm{T}}\mathbf{y} + \sum_{h=1}^{s} p_h f_h^{cv}(\mathbf{x}_h, \mathbf{q}_h; \boldsymbol{\omega}_h) & & \\
\text{s.t.} \quad & \mathbf{A}\mathbf{y} \leq \mathbf{b}, & & \\
& \mathbf{B}_h\mathbf{y} + \mathbf{g}_h^{cv}(\mathbf{x}_h, \mathbf{q}_h; \boldsymbol{\omega}_h) \leq \mathbf{0}, & \forall h \in \{1,\ldots,s\}, & \quad \text{(LBP)} \\
& \mathbf{y} \in \boldsymbol{Y}, & & \\
& (\mathbf{x}_h, \mathbf{q}_h) \in \boldsymbol{D}_h, & \forall h \in \{1,\ldots,s\} &
\end{aligned}$$

Problem LBP is a two-stage stochastic MICP thus GBD can be applied with the corresponding subproblems termed the the Master Problem (MP), the Primal Bounding Problem (PBP) and PBP subproblems, the Feasibility Problem (FP) and FP subproblems, the Relaxed Master Problem (RMP) and the Feasibility Relaxed Master Problem (FRMP) as presented next.

The Master Problem (MP), Primal Bounding Problem (PBP) and PBP subproblems

From Problem LBP, a similar partitioning approach to that presented in Section 5 is implemented. Analogously to Problem SMILP-PART, we define Problem LBP-PART which only searches over the space of $\mathbf{y}$ variables and whose objective function is defined implicitly in terms of the optimal values of embedded optimization problems $\mathrm{PBP}_h(\mathbf{y})$ for all $h \in \{1,\ldots,s\}$. The

NLP subproblems $\text{PBP}_h(\mathbf{y})$ (analogous to problems $\text{LP}_h(\mathbf{y})$) are termed the PBP subproblems where the Primal Bounding Problem (PBP) collects their optimal objective function values as presented in Equation PBP($\mathbf{y}$) (defined on feasible $\mathbf{y}$ values).

$$\begin{aligned}
\min_{\mathbf{y}} \quad & \mathbf{c}^{\mathrm{T}}\mathbf{y} + \sum_{h=1}^{s} v_h(\mathbf{y}) \\
\text{s.t.} \quad & \mathbf{y} \in \boldsymbol{V} \equiv \Big\{ \mathbf{y} \in \boldsymbol{Y} : \mathbf{A}\mathbf{y} \leq \mathbf{b} \text{ and} \\
& \qquad \exists (\mathbf{x}_h, \mathbf{q}_h) \in \boldsymbol{D}_h : \mathbf{g}_h^{cv}(\mathbf{x}_h, \mathbf{q}_h; \boldsymbol{\omega}_h) \leq -\mathbf{B}_h\mathbf{y}, \forall h \in \{1, \ldots, s\} \Big\} \subset \boldsymbol{Y}
\end{aligned} \tag{LBP-PART}$$

$$\begin{aligned}
v_h(\mathbf{y}) \quad = \quad & \min_{\mathbf{x}_h, \mathbf{q}_h} \quad p_h f_h^{cv}(\mathbf{x}_h, \mathbf{q}_h; \boldsymbol{\omega}_h) \\
& \text{s.t.} \quad \mathbf{g}_h^{cv}(\mathbf{x}_h, \mathbf{q}_h; \boldsymbol{\omega}_h) \leq -\mathbf{B}_h\mathbf{y}, \\
& \qquad (\mathbf{x}_h, \mathbf{q}_h) \in \boldsymbol{D}_h,
\end{aligned} \tag{$\text{PBP}_h(\mathbf{y})$}$$

$$v(\mathbf{y}) \quad = \quad \mathbf{c}^{\mathrm{T}}\mathbf{y} + \sum_{h=1}^{s} v_h(\mathbf{y}) \tag{PBP($\mathbf{y}$)}$$

Remarks and Reformulations:

1. The Problems $\text{PBP}_h(\mathbf{y})$ are convex NLPs. The size of each problem is independent of the number of scenarios. We assume that these convex programs can either be solved to global optimality with a standard NLP solver for a given value of $\mathbf{y}$ or are infeasible. If an optimal solution $(\hat{\mathbf{x}}_h, \hat{\mathbf{q}}_h)$ is found, we assume that the NLP solver also provides the associated duality multiplier $(\hat{\boldsymbol{\lambda}}_h)$ which is known to exist since each of the problems is convex. If any of the Problems $\text{PBP}_h(\mathbf{y})$ are infeasible, a related Feasibility Problem can be constructed and solved as discussed in the next section.
2. Problems LBP-PART and LBP have the same objective function. However, Problem LBP-PART is a substantially smaller problem since it only searches over the space of the $\mathbf{y}$ variables.

3. The trade-off is that the objective function of Problem LBP-PART is defined implicitly and, for each candidate value $\mathbf{y}$, requires the solutions of all the NLP problems $\text{PBP}_h(\mathbf{y})$ parameterized by that $\mathbf{y}$. This is computationally intractable. Instead, a duality theory-based reformulation is used as explained next:

   - First, since Problems $\text{PBP}_h(\mathbf{y})$ are all convex, strong duality holds thus we can rewrite:

$$v_h(\mathbf{y}) = \sup_{\boldsymbol{\lambda}_h \geq \mathbf{0}} \inf_{(\mathbf{x}_h, \mathbf{q}_h) \in \boldsymbol{D}_h} \Big\{ p_h f_h^{cv}(\mathbf{x}_h, \mathbf{q}_h; \boldsymbol{\omega}_h) + \boldsymbol{\lambda}_h{}^{\mathrm{T}} (\mathbf{g}_h^{cv}(\mathbf{x}_h, \mathbf{q}_h; \boldsymbol{\omega}_h) + \mathbf{B}_h \mathbf{y}) \Big\}$$

   - We can then re-write the Primal Bounding Problem (Equation PBP($\mathbf{y}$)):

$$v(\mathbf{y}) = \mathbf{c}^{\mathrm{T}}\mathbf{y} + \sum_{h=1}^{s} \sup_{\boldsymbol{\lambda}_h \geq \mathbf{0}} \inf_{(\mathbf{x}_h, \mathbf{q}_h) \in \boldsymbol{D}_h} \Big\{ p_h f_h^{cv}(\mathbf{x}_h, \mathbf{q}_h; \boldsymbol{\omega}_h) + \boldsymbol{\lambda}_h{}^{\mathrm{T}} (\mathbf{g}_h^{cv}(\mathbf{x}_h, \mathbf{q}_h; \boldsymbol{\omega}_h) + \mathbf{B}_h \mathbf{y}) \Big\}$$

   - Using the definition of the supremum, the above expression can be translated into the following form which gives an infinite number of constraints:

$$v(\mathbf{y}) \geq \mathbf{c}^{\mathrm{T}}\mathbf{y} + \sum_{h=1}^{s} \inf_{(\mathbf{x}_h, \mathbf{q}_h) \in \boldsymbol{D}_h} \Big\{ p_h f_h^{cv}(\mathbf{x}_h, \mathbf{q}_h; \boldsymbol{\omega}_h) + \boldsymbol{\lambda}_h{}^{\mathrm{T}} (\mathbf{g}_h^{cv}(\mathbf{x}_h, \mathbf{q}_h; \boldsymbol{\omega}_h) + \mathbf{B}_h \mathbf{y}) \Big\},$$
$$\forall (\boldsymbol{\lambda_1}, \ldots, \boldsymbol{\lambda_s}) \in \mathbb{R}_+^{m_h^{cv} \times s}$$

     where m_h^{cv} is the number of second-stage constraints in each scenario for Problem LBP.

   - In the equation above, every possible vector $(\boldsymbol{\lambda_1}, \ldots, \boldsymbol{\lambda_s})$ belonging to the infinite set $\mathbb{R}_+^{m_h^{cv} \times s}$ gives rise to a new constraint. Thus, each vector of values $(\boldsymbol{\lambda_1}, \ldots, \boldsymbol{\lambda_s})$ can be used as an index for the constraint set, and we define a function $\Big(\mathbf{y}, (\boldsymbol{\lambda_1}, \ldots, \boldsymbol{\lambda_s})\Big)$ to represent a single one of these constraints (termed a "Benders Optimality cut") i.e.,

$$\Big(\mathbf{y}, (\boldsymbol{\lambda_1}, \ldots, \boldsymbol{\lambda_s})\Big) \equiv \mathbf{c}^{\mathrm{T}}\mathbf{y} \; +$$
$$\sum_{h=1}^{s} \inf_{(\mathbf{x}_h, \mathbf{q}_h) \in \boldsymbol{D}_h} \Big\{ p_h f_h^{cv}(\mathbf{x}_h, \mathbf{q}_h; \boldsymbol{\omega}_h) + \boldsymbol{\lambda}_h{}^{\mathrm{T}} (\mathbf{g}_h^{cv}(\mathbf{x}_h, \mathbf{q}_h; \boldsymbol{\omega}_h) + \mathbf{B}_h \mathbf{y}) \Big\},$$

4. Another issue with Problem LBP-PART is that testing the second membership condition of each $\mathbf{y}$ in the feasible set $\boldsymbol{V}$ is also computationally expensive. Thus, a similar reformulation is implemented to replace this condition with an (infinite) number of constraints that would exclude infeasible $\mathbf{y}$ values. Duality theory once again provides a useful result presented in Theorem 5 that allows for this reformulation. We note that similar to Dual Problem, Theorem 5 also has a geometric interpretation obtained by formulating the image space representation of the constraint functions $\mathbf{g}_h^{cv}$ as presented in [57, 58]. Each function $\Big(\mathbf{y}, (\boldsymbol{\mu}_1, \ldots, \boldsymbol{\mu}_s)\Big)$ also defines a single constraint (termed a "Benders Feasibility cut") and the vector $(\boldsymbol{\mu}_1, \ldots, \boldsymbol{\mu}_s)$ provides an index for the constraint set.
5. The last reformulation of Problem LBP-PART is for convenience: The objective function is defined in terms of a dummy decision variable $\eta \in \mathbb{R}$. Since Problem LBP-PART is a minimization problem, the constraint below becomes active at the optimum.

$$\eta \geq \mathbf{c}^{\mathrm{T}}\mathbf{y} + \sum_{h=1}^{s} v_h(\mathbf{y})$$

[Dual representation of second membership condition of set $\boldsymbol{V}$] Consider a point $\mathbf{y} \in \boldsymbol{Y}$. The set $\boldsymbol{D}_h$ is convex and functions $\mathbf{g}_h^{cv}$ are convex on $\boldsymbol{D}_h$ (as constructed).

If there exists $(\mathbf{x}_h, \mathbf{q}_h) \in \boldsymbol{D}_h : \mathbf{g}_h^{cv}(\mathbf{x}_h, \mathbf{q}_h; \boldsymbol{\omega}_h) \leq -\mathbf{B}_h\mathbf{y}$, $\forall h \in \{1, \ldots, s\}$

$$\Longleftrightarrow$$

$\mathbf{y}$ satisfies the set of inequalities: $\Big(\mathbf{y}, (\boldsymbol{\mu}_1, \ldots, \boldsymbol{\mu}_s)\Big) \leq \mathbf{0}$, $\forall (\boldsymbol{\mu}_1, \ldots, \boldsymbol{\mu}_s) \in \boldsymbol{M}$

where:

$$\Big(\mathbf{y}, (\boldsymbol{\mu}_1, \ldots, \boldsymbol{\mu}_s)\Big) \equiv \sum_{h=1}^{s} \inf_{(\mathbf{x}_h, \mathbf{q}_h) \in \boldsymbol{D}_h} \Big\{ {\boldsymbol{\mu}_h}^{\mathrm{T}} (\mathbf{g}_h^{cv}(\mathbf{x}_h, \mathbf{q}_h; \boldsymbol{\omega}_h) + \mathbf{B}_h \mathbf{y}) \Big\},$$

$$\boldsymbol{M} \equiv \left\{ (\boldsymbol{\mu}_1, \ldots, \boldsymbol{\mu}_s) \in \mathbb{R}_+^{m_h^{cv} \times s} : \boldsymbol{\mu}_1, \ldots, \boldsymbol{\mu}_s \geq \mathbf{0}, \sum_{h=1}^{s} \sum_{i=1}^{m_h^{cv}} \mu_{h,i} = 1 \right\}.$$

With the above reformulations, Problem LBP-PART can be rewritten as Problem MP which is termed the Master Problem:

$$\begin{array}{ll} \min\limits_{\eta, \mathbf{y}} & \eta \\ \text{s.t.} & \mathbf{A}\mathbf{y} \leq \mathbf{b}, \\ & \eta \geq \Big(\mathbf{y}, (\boldsymbol{\lambda_1}, \ldots, \boldsymbol{\lambda_s})\Big), \ \forall (\boldsymbol{\lambda_1}, \ldots, \boldsymbol{\lambda_s}) \in \mathbb{R}_+^{m_h^{cv} \times s} \\ & \mathbf{0} \geq \Big(\mathbf{y}, (\boldsymbol{\mu}_1, \ldots, \boldsymbol{\mu}_s)\Big), \ \forall (\boldsymbol{\mu}_1, \ldots, \boldsymbol{\mu}_s) \in \boldsymbol{M} \\ & \mathbf{y} \in \boldsymbol{Y}, \eta \in \mathbb{R} \end{array} \tag{MP}$$

The Feasibility Problem (FP) and FP subproblems

If any of the PBP subproblems is infeasible, a related Feasibility Problem FP($\mathbf{y}$) is solved which in turn decomposes to solving an FP subproblem FP$_h$($\mathbf{y}$) for each scenario h. In each of these subproblems, a slack variable vector $\mathbf{z}_h$ is introduced and the objective is to minimize the violation of the constraints (according to an appropriate norm). We note that problems FP$_h$($\mathbf{y}$) are convex programs since any norm function is convex. Thus, we assume they can be solved to global optimality using an NLP solver that also provides an associated duality multiplier (denoted $\hat{\boldsymbol{\mu}}_h$). The set of duality multipliers from all the FP subproblems provides useful information as discussed in the next section on the Relaxed Master Problem.

$$r(\mathbf{y}) \quad = \quad \sum_{h=1}^{s} r_h(\mathbf{y}) \tag{FP($\mathbf{y}$)}$$

$$
\begin{aligned}
r_h(\mathbf{y}) \quad = \quad & \min_{\mathbf{x}_h, \mathbf{q}_h, \mathbf{z}_h} \quad p_h \|\mathbf{z}_h\| \\
& \text{s.t.} \qquad \mathbf{g}_h^{cv}(\mathbf{x}_h, \mathbf{q}_h; \boldsymbol{\omega}_h) + \mathbf{B}_h \mathbf{y} \leq \mathbf{z}_h, \\
& \qquad\quad (\mathbf{x}_h, \mathbf{q}_h) \in \boldsymbol{D}_h, \mathbf{z}_h \in \boldsymbol{Z}_h
\end{aligned}
\tag{$\mathrm{FP}_h(\mathbf{y})$}
$$

The Relaxed Master Problem (RMP)

Problem MP is still computationally challenging to solve as it is a semi-infinite problem since it has an infinite number of constraints. This motivates the construction of a Relaxed Master Problem (Problem RMP) where only a finite subset of these constraints is iteratively added.

The following features of Problem RMP are presented:

- The finite index sets T and S are introduced: Each element j of T indexes a single Benders Optimality cut while each element i of S indexes a single Benders Feasibility cut . Thus, the elements j and s correspond to the sets of vectors $(\boldsymbol{\lambda_1}, \ldots, \boldsymbol{\lambda_s})$ and $(\boldsymbol{\mu}_1, \ldots, \boldsymbol{\mu}_s)$ respectively. At the start of the NGBD algorithm, the sets T and S are empty and one constraint is added to one of the sets at each iteration.

- Since Problem RMP is a relaxation of Problem MP (which is in turn a relaxation of Problem SP), its optimal objective function value provides a rigorous lower bound (LBD) for the two-stage stochastic program by the Lower Bounding Principle. We also note that since Problem RMP gets more constrained as more cuts are added at each iteration, this LBD is guaranteed to increase or remain the same.

- The overall strategy is to repeatedly solve Problem RMP with an increasing number of constraints. After each iteration, suppose $(\hat{\eta}, \hat{\mathbf{y}})$ is the optimal solution of Problem RMP, the next step is to test if any of the constraints left out from Problem MP are violated by this optimal solution. One crucial feature of the NGBD algorithm is that this test can be performed cheaply by solving subproblems $\mathrm{PBP}_h(\mathbf{y})$ with $\mathbf{y}$ fixed to be $\hat{\mathbf{y}}$. If the optimal solutions for all the PBP subproblems are found and $\hat{\eta} < v(\hat{\mathbf{y}})$, then it can be shown that (at least) one of the constraints of Problem MP has been violated. The intuition for the above test is as follows: If $(\hat{\eta}, \hat{\mathbf{y}})$ did not violate any constraints of Problem MP, then as a result of strong duality, $v(\hat{\mathbf{y}})$ should be equal to $\hat{\eta}$.

Thus, failure of this test implies that a Benders Optimality cut should be added to Problem RMP. Advantageously, the derivation of this cut can also be done efficiently if the NLP solver for subproblems $\text{PBP}_h(\mathbf{y})$ provides duality multipliers ($\hat{\boldsymbol{\lambda}}_h$) (which exist for convex programs): Applying the definition of a duality multiplier, we can write:

$$v_h(\hat{\mathbf{y}}) = \inf_{(\mathbf{x}_h, \mathbf{q}_h) \in \boldsymbol{D}_h} \left\{ p_h f_h^{cv}(\mathbf{x}_h, \mathbf{q}_h; \boldsymbol{\omega}_h) + (\hat{\boldsymbol{\lambda}}_h)^{\mathrm{T}} (\mathbf{g}_h^{cv}(\mathbf{x}_h, \mathbf{q}_h; \boldsymbol{\omega}_h) + \mathbf{B}_h \hat{\mathbf{y}}) \right\}$$

Thus:

$$v(\hat{\mathbf{y}}) = \mathbf{c}^{\mathrm{T}} \hat{\mathbf{y}} + \sum_{h=1}^{s} \inf_{(\mathbf{x}_h, \mathbf{q}_h) \in \boldsymbol{D}_h} \left\{ p_h f_h^{cv}(\mathbf{x}_h, \mathbf{q}_h; \boldsymbol{\omega}_h) + (\hat{\boldsymbol{\lambda}}_h)^{\mathrm{T}} (\mathbf{g}_h^{cv}(\mathbf{x}_h, \mathbf{q}_h; \boldsymbol{\omega}_h) + \mathbf{B}_h \hat{\mathbf{y}}) \right\}$$

We can then re-write the Benders Optimality cut indexed by the set of duality multipliers $(\hat{\boldsymbol{\lambda}}_1, \ldots, \hat{\boldsymbol{\lambda}}_s)$ as:

$$\left(\mathbf{y}, (\hat{\boldsymbol{\lambda}}_1, \ldots, \hat{\boldsymbol{\lambda}}_s) \right) \equiv v(\hat{\mathbf{y}}) + \mathbf{c}^{\mathrm{T}} (\mathbf{y} - \hat{\mathbf{y}}) + \sum_{h=1}^{s} (\hat{\boldsymbol{\lambda}}_h)^{\mathrm{T}} \mathbf{B}_h (\mathbf{y} - \hat{\mathbf{y}})$$

A more rigorous argument for using the above set of duality multipliers is provided in [12].

- Conversely, if any of Problems $\text{PBP}_h(\mathbf{y})$ (with $\mathbf{y}$ fixed to be $\hat{\mathbf{y}}$) is infeasible, then $\hat{\mathbf{y}}$ violates one of the Benders Feasibility cuts of Problem MP. Without proof, we mention that the set of duality multipliers obtained from solution of problems $\text{FP}_h(\mathbf{y})$ (with $\mathbf{y}$ fixed to be $\hat{\mathbf{y}}$) denoted $(\hat{\boldsymbol{\mu}}_1, \ldots, \hat{\boldsymbol{\mu}}_s)$ provides an index for one violated Benders Feasibility cut. A similar derivation as above gives the following constraint which is guaranteed to make the current solution $\hat{\mathbf{y}}$ infeasible in the next iteration of Problem RMP:

$$\left(\mathbf{y}, (\hat{\boldsymbol{\mu}}_1, \ldots, \hat{\boldsymbol{\mu}}_s) \right) \equiv r(\hat{\mathbf{y}}) + \sum_{h=1}^{s} (\hat{\boldsymbol{\mu}}_h)^{\mathrm{T}} \mathbf{B}_h (\mathbf{y} - \hat{\mathbf{y}})$$

- In summary, at each iteration either a Benders Optimality or Feasibility cut is added to Problem RMP by appending a set of duality multipliers to either set T or S obtained from the PBP or the FP.

- The last set of integer cuts (also termed "Balas cuts" as detailed in [27]) is required for guaranteed convergence of the NGBD algorithm but not for the GBD or BD algorithms. The point of these cuts is to explicitly prevent the NGBD algorithm from cycling back to previously visited $\mathbf{y}$ values in prior iterations of Problem RMP. The sets O^t and Z^t are defined as follows: $O^t \equiv \{l \in \{1, \cdots, n_y\} : y_l^t = 1\}, Z^t \equiv \{l \in \{1, \cdots, n_y\} : y_l^t = 0\}$.

$$
\begin{aligned}
\min_{\eta, \mathbf{y}} \quad & \eta \\
\text{s.t.} \quad & \mathbf{A}\mathbf{y} \leq \mathbf{b}, \\
& \eta \geq v(\hat{\mathbf{y}}^j) + \mathbf{c}^{\mathrm{T}}(\mathbf{y} - \hat{\mathbf{y}}^j) + \sum_{h=1}^{s} (\hat{\boldsymbol{\lambda}}_h^j)^{\mathrm{T}} \mathbf{B}_h (\mathbf{y} - \hat{\mathbf{y}}^j), \ \ \forall j \in T, \\
& \mathbf{0} \geq r(\hat{\mathbf{y}}^i) + \sum_{h=1}^{s} (\hat{\boldsymbol{\mu}}_h^i)^{\mathrm{T}} \mathbf{B}_h (\mathbf{y} - \hat{\mathbf{y}}^i), \ \ \forall i \in S, \\
& |O^t| - 1 \ \geq \sum_{l \in O^t} y_l - \sum_{l \in Z^t} y_l, \ \ \forall t \in T \cup S, \\
& \mathbf{y} \in \boldsymbol{Y}, \eta \in \mathbb{R}
\end{aligned}
\tag{RMP}
$$

The Feasibility Relaxed Master Problem (FRMP)

For early iterations of the NGBD algorithm, the set T may be empty. In this case, it may be necessary to solve an auxiliary problem termed the Feasibility Relaxed Master Problem (Problem FRMP) to obtain a feasible value of $\mathbf{y}$:

$$
\begin{aligned}
\min_{\mathbf{y}} \quad & \|\mathbf{y}\| \\
\text{s.t.} \quad & \mathbf{A}\mathbf{y} \leq \mathbf{b}, \\
& \mathbf{0} \geq r(\hat{\mathbf{y}}^i) + \sum_{h=1}^{s} (\hat{\boldsymbol{\mu}}_h^i)^{\mathrm{T}} \mathbf{B}_h (\mathbf{y} - \hat{\mathbf{y}}^i), \ \ \forall i \in S, \\
& |O^t| - 1 \ \geq \sum_{l \in O^t} y_l - \sum_{l \in Z^t} y_l, \ \ \forall t \in S, \\
& \mathbf{y} \in \boldsymbol{Y}
\end{aligned}
\tag{FRMP}
$$

Upper Bounding with the Primal Problem (PP) and PP subproblems

The procedure to generate upper bounds (UBD) for Problem SP involves solving a Primal Problem (Problem PP($\hat{\mathbf{y}}$)) formulated by restricting the $\mathbf{y}$ variables to the optimal solution values $\hat{\mathbf{y}}$ obtained from solving Problem RMP at each iteration. This problem naturally decomposes into solving s PP subproblems PP$_h(\hat{\mathbf{y}})$:

$$u(\hat{\mathbf{y}}) \quad = \quad \mathbf{c}^{\mathrm{T}}\hat{\mathbf{y}} + \sum_{h=1}^{s} u_h(\hat{\mathbf{y}}) \tag{PP($\hat{\mathbf{y}}$)}$$

$$\begin{aligned} u_h(\hat{\mathbf{y}}) \quad = \quad & \min_{\mathbf{x}_h} \quad p_h f_h(\mathbf{x}_h; \boldsymbol{\omega}_h) \\ & \text{s.t.} \quad \mathbf{g}_h(\mathbf{x}_h; \boldsymbol{\omega}_h) \leq -\mathbf{B}_h\hat{\mathbf{y}}, \\ & \qquad \mathbf{x}_h \in \boldsymbol{X}_h, \end{aligned} \tag{PP$_h(\hat{\mathbf{y}})$}$$

We note that even though the PP subproblems are of a lower dimension than the PBP subproblems, their solution is typically the most expensive part of the NGBD algorithm because they are nonconvex NLPs. Thus, global optimization strategies such as spatial branch-and-bound are relevant for these nonconvex programs. To improve the performance of the algorithm, the following options can also be considered:

1. Instead of solving Problems PP$_h(\hat{\mathbf{y}})$ immediately after a candidate $\hat{\mathbf{y}}$ vector is available, the lower bounding loop (consisting of Problems RMP and PBP$_h(\mathbf{y})$/FP$_h(\mathbf{y})$) can first be converged to give an optimal solution to Problem LBP. After this, Problem PP$_h(\hat{\mathbf{y}})$ can be solved with this candidate vector $\hat{\mathbf{y}}$ that is optimal for Problem LBP. This strategy minimizes the number of Problems PP$_h(\hat{\mathbf{y}})$ solved.
2. It may also be more efficient to to accept a good local optimum or even a feasible solution for Problem PP($\hat{\mathbf{y}}$) as both of these provides rigorous UBDs. The trade-off is that the UBD attained is higher than that attained with a global optimum. In addition, with this strategy, there are no guarantees that the algorithm converges to a global optimal solution of Problem SP (although the algorithm still converges because of the inclusion of Balas cuts).
3. Problems PP$_h(\hat{\mathbf{y}})$ may also be solved in parallel on a multi-core computer.

Algorithm Summary and Remarks

After convexifying the original stochastic MINLP, the lower bounding loop of the NGBD algorithm first begins with solving a decomposable Primal Bounding Problem with an initial guess for the $\mathbf{y}$ variables. If this problem is feasible, an upper bound for the lower bounding problem is updated and the duality multipliers attained are used to generate Benders Optimality cuts for the Relaxed Master Problem. If any of the decomposed problems is infeasible, a Feasibility Problem is solved and the duality multipliers attained are used to generate Benders Feasibility cuts for the Relaxed Master Problem. The Relaxed Master Problem is derived by relaxing the constraints of the Master Problem. This Master Problem in turn is derived by partitioning (projection) of the convexified problem onto the space of the $\mathbf{y}$ variables, and replacing the embedded optimization problem (in the $\mathbf{x}$ space) with an infinite number of constraints by leveraging its dual representation. Similarly, a dual representation is utilized to define the set of feasible $\mathbf{y}$ values. The Relaxed Master Problem provides a lower bound and its solution gives the $\mathbf{y}$ value used for the next iteration of the Primal Bounding Problems. Once the lower bounding loop has converged, a decomposable Primal Problem is solved by fixing the $\mathbf{y}$ values to the optimal values attained from the Relaxed Master Problem. A feasible or optimal solution of the Primal Problem provides an upper bound. Affine inequalities are added to the Relaxed Master Problem to exclude previously visited solutions $\mathbf{y}$ and the procedure is iterated until convergence.

The NGBD algorithm scales favorably with respect to one dimension of problem size: the total number of scenarios. The reasoning for this property is as follows:

- The partitioning and dualizing procedures imply that the sizes of all of the problems solved are independent of the number of scenarios. Thus, solving several smaller problems is computationally advantageous over solving fewer large problems.

- It is empirically observed that when the convex relaxations are tight, the NGBD algorithm only takes a few iterations to converge. Additionally, the number of Primal Problems solved is usually much smaller than the number of Relaxed Master Problems solved.

Supplementary Material 2:

Complete optimization under uncertainty model

Key decision variables

The key design (denoted by vector $\mathbf{y}$) and operational decision variables in scenario h (denoted by vector $\mathbf{x}_h$) are presented in the main text.

List of Process Sections

The flexible polygeneration system studied consists of 20 process sections. Let U denote the set of all process sections consisting of elements u (as presented in Table 6). Each process section is associated with a representative extensive variable termed the "characteristic throughput" in scenario h ($F_{u,h}$).

	Process Section, u	**Abbreviation**	**Characteristic throughput** ($F_{u,h}$)	**Stream**	**Units**
	Waste Tire Train				
1.	Aggregate Waste Tire converter	TAGG	Mass flow of tire	$m_{tire,h}$	kg/s tire
2.	Air Separation Unit	ASU	Mass flow of O_2	$m_{ASU,O_2,h}$	kg/s O_2
	Product train - (Synthetic) Natural gas				
3.	SNG train - Water Gas Shift 1	WGS1	Extent of conversion of CO	$\xi_{METHWGS,h}$	kmol/s CO
4.	SNG train - Selexol 1 CO_2 removal	SEL1	Mole flow of CO_2 in	$f_{WGS1\_prod,i,h}$	kmol/s CO_2
5.	Methanation	METH	Mass flow of feed in	$m_{METH\_in,h}$	kg/s tire-derived syngas
6.	(Synthetic or well) NG Liquefaction	LIQ	Mass flow of (S)NG	$m_{LNG,h}$	kg/s LNG
7.	Aggregate Natural gas converter	NGAGG	Mass flow of natural gas to reformer	$m_{NGRef,h}$	kg/s natural gas
	Product train - Methanol, DME and olefins				
8.	MeOH train -Water Gas Shift 2	WGS2	Extent of conversion of CO	$\xi_{MEOHWGS,h}$	kmol/s CO
9.	MeOH train - Selexol 2 CO_2 removal	SEL2	Mole flow of CO_2 in	$f_{MEOH\_Blended,CO_2,h}$	kmol/s CO_2
10.	Methanol synthesis & purification	MEOH	Mass flow of feed in	$m_{MEOH\_in,h}$	kg/s syngas
11.	DME synthesis	DME	Mass flow of MeOH in	$m_{MeOH\_ToDME,h}$	kg/s MeOH
12.	Methanol to Olefins	MTO	Mass flow of MeOH in	$m_{MeOH\_ToMTO,h}$	kg/s MeOH
	Product train - Power generation				
13.	Gas Turbine	GT	Work output	$W_{GT,h}$	MW
14.	HRSG	HRSG	Heat recovered	$Q_{HQ\_HRSG,h}$	MW
15.	Steam Turbine	ST	Work output	$W_{ST,h}$	MW
16.	Electric Plant Accessories	EACC	Total work output	$W_{GT,h} + W_{ST,h}$	MW
	CO_2 capture and miscellaneous				
17.	DGA CO_2 removal	DGA	Mass flow of CO_2 in	$m_{DGA,CO_2,h}$	kg/s CO_2
18.	CO_2 compression, liquefaction & sequestration	SEQ	Mass flow of CO_2 sequestered	$m_{CCS,CO_2,h}$	kg/s CO_2
19.	Miscellaneous [1]	MISC	Total thermal input	$TI_{LHV,h}$	MW LHV
20.	Water systems [2]	H2O	Total cooling duty	$Q_{CW\_net,h}$	MW

Table 6: Process sections included in polygeneration system. [1] Miscellaneous includes Instrumentation & control, Site preparation & improvement and Building & structures. [2] Water systems include cooling water systems, feed water and BOP water systems. We note that where relevant the mole flow rates listed above denote the mole flows of the relevant component only without including impurities.

Feedstock characterization

Waste Tire

The waste tire feedstock has a composition and lower heating value (LHV_{tire}) presented in Table 7.

Ultimate Analysis (Ult)	**wt %**	**Proximate Analysis**	**wt %**
C	77.3	Volatile Matter (VM)	67.7
H	6.2	Fixed Carbon (FC)	25.5
N	0.6	Ash	6.8
S	1.8		
O	7.3		
Ash	6.8		
LHV_{tire} [MJ/kg]	33.96		

Table 7: Characterization of waste tire

Natural Gas

The composition and feedstock specification for natural gas are presented in Table 8.

Composition	**(mol %)**	**Conditions**	
CH_4	93.9	Pressure	30 bar
CO_2	0.01	Temperature	30 °C
C_2H_6	0.032		
C_3H_8	0.007		
$C_4{}^+$	0.004		
N_2	0.008		
LHV_{NG} [MJ/kg]	47.84		

Table 8: Characterization of Natural Gas [29]

Mass balance model

Let I denote the set of components relevant to the surrogate mass balance model. The components $i \in I$ are presented in Table 9, where MW_i denotes the molecular weight of component i (obtained from Aspen Plus data banks).

	Component, i	MW_i [kg/kmol]	**Component type**
1.	CO	28.010	Conventional
2.	CO_2	44.010	Conventional
3.	H_2	2.016	Conventional
4.	CH_4	16.043	Conventional
5.	H_2O	18.015	Conventional
6.	N_2	28.013	Conventional
7.	O_2	31.999	Conventional
8.	NH_3	17.031	Conventional
9.	H_2S	34.082	Conventional
10.	COS	60.076	Conventional
11.	Cl_2	70.905	Conventional
12.	HCl	36.461	Conventional
13.	NO	30.006	Conventional
14.	NO_2	46.006	Conventional
15.	SO_2	64.065	Conventional
16.	SO_3	80.064	Conventional
17.	CH_3OH	32.042	Conventional
18.	C	12.011	Solid
19.	S	32.066	Solid

Table 9: Components involved in the surrogate mass balance model. The settings used for the components in Aspen Plus are presented as well.

We note that there are several additional components not listed here which are included in the Aspen Plus simulation. In the following sections, we present the mass balance surrogate models implemented. We note that for any stream in the surrogate model, any molar flow rates for components i not defined explicitly can be taken to be 0.000 [kmols/s].

Aggregate Waste tire gasifier

The aggregate waste tire gasifier encompasses the following units: Tire feedstock and slurry preparation unit, entrained flow gasifier, syngas cleaning (scrubber, COS hydrolysis, syngas cooler, sour water knockout drum, Selexol-based H_2S removal unit, Claus unit) and the ash handling system. Detailed descriptions of these units and the simulation strategy are presented in our previous work [3, 4, 43]. The clean tire-derived syngas mole flow rate in scenario h ($f_{TDsweet\_gas,i,h}$) is a linear function of feed flow rate of tire $m_{tire,h}$. The mole fraction of component i belonging to the component set I ($x_{TDsweet\_gas,i}$) is regressed from the Aspen Plus simulation with the coeffi-

Component, i	$x_{TDsweet\_gas,i}$
CO	0.542
CO_2	0.071
H_2	0.381
CH_4	0.006

Table 10: The mole fractions of each relevant component i in tire-derived syngas obtained from the rigorous Aspen Plus simulation

cients presented in Table 10. The term $\frac{R_{ST}}{MW_{TDsweet\_gas}}$ (where $MW_{TDsweet\_gas}$ is the molecular weight of syngas and R_{ST} is the ratio of the mass flow rates of clean syngas to tire) is also determined from the simulation to be 0.103 [$\text{kmols}^{-1}_{TDsweet\_gas}/\text{kgs}^{-1}_{tire}$].

$$f_{TDsweet\_gas,i,h} = \frac{x_{TDsweet\_gas,i} \cdot R_{ST} \cdot m_{tire,h}}{MW_{TDsweet\_gas}},\ \forall i \in I, \forall h \in \{1, ..., s\} \quad (12)$$

The mass of sulfur product from the Claus process $m_{CLAUS,\text{S},h}$ [kg/s] is also regressed from the simulation with the corresponding coefficient R_{Sulfur} determined to be 0.016 [$\text{kg}_{sulfur}/\text{kg}_{tire}$] :

$$m_{CLAUS,\text{S},h} = R_{Sulfur} \cdot m_{tire,h}, \forall h \in \{1, ..., s\}, \quad (13)$$

Tire-derived syngas splitter

The tire-derived syngas is preheated and then heads to one of three downstream synthesis sections: Methanation, methanol synthesis or the gas turbine section. The corresponding split fraction of tire-derived syngas to each of these three sections (denoted $S_{TSNG,h}$, $S_{TMeOH,h}$ and $S_{TGT,h}$ respectively) is a decision variable, thus the molar flow rates of the corresponding streams are given by Equation 14, where $f_{TMETH\_feed,i,h}$, $f_{TMEOH\_feed,i,h}$ and $f_{TGT\_feed,i,h}$ [kmol/s] denote the molar flow rates of component i in the tire-derived syngas streams heading to the methanation, methanol synthesis and gas turbine sections respectively in scenario h.

$$
\begin{gathered}
f_{TMETH\_feed,i,h} = f_{TDsweet\_gas,i,h} \cdot S_{TSNG,h},\ \forall i \in I, \forall h \in \{1, ..., s\} \\
f_{TGT\_feed,i,h} = f_{TDsweet\_gas,i,h} \cdot S_{TGT,h},\ \forall i \in I, \forall h \in \{1, ..., s\} \\
f_{TMEOH\_feed,i,h} = f_{TDsweet\_gas,i,h} \cdot S_{TMeOH,h},\ \forall i \in I, \forall h \in \{1, ..., s\} \\
S_{TSNG,h} + S_{TGT,h} + S_{TMeOH,h} = 1.0, \forall h \in \{1, ..., s\}
\end{gathered} \tag{14}
$$

Natural gas feedstock splitter

The natural gas feedstock of mass $m_{NG,h}$ [kg/s] is split into three branches heading to the natural gas reforming, gas turbine and liquefaction sections according to split fractions $S_{NGRef,h}$, $S_{NGGT,h}$, $S_{NGLiq,h}$ respectively. The material balance constraints for the natural gas splitter are given by Equation 15 where $m_{NGRef,h}$, $m_{NGGT,h}$ and $m_{NGLiq,h}$ [kg/s] denote the mass flow rates of natural gas heading to the reforming, gas turbine and liquefaction sections respectively in scenario h.

$$
\begin{gathered}
m_{NGRef,h} = m_{NG,h} \cdot S_{NGRef,h}, \forall h \in \{1, ..., s\} \\
m_{NGGT,h} = m_{NG,h} \cdot S_{NGGT,h}, \forall h \in \{1, ..., s\} \\
m_{NGLiq,h} = m_{NG,h} \cdot S_{NGLiq,h}, \forall h \in \{1, ..., s\} \\
S_{NGRef,h} + S_{NGGT,h} + S_{NGLiq,h} = 1.0, \forall h \in \{1, ..., s\}
\end{gathered} \tag{15}
$$

Liquified (S)NG train - Water Gas Shift 1

Tire-derived syngas heading to the methanation section can be upgraded by diverting a portion of the stream to a WGS reactor. The overall conversion in scenario h ($c_{SNGWGS,h}$) is a decision variable . The water gas shift reaction is presented in Equation 16, with the corresponding stoichiometric coefficient of component i is denoted by $\nu_{i,WGS}$.

$$
\mathrm{CO} + \mathrm{H_2O} \rightleftharpoons \mathrm{H_2} + \mathrm{CO_2} \tag{16}
$$

We assume that a stoichiometric amount of steam is used. Thus, the molar flow rate of the steam stream ($f_{WGS1\_steam,\mathrm{H_2O},h}$) is equal to the extent

of the WGS reaction ($\xi_{METHWGS,h}$ [kmol/s]) as shown in Equation 17. The term $f_{WGS1\_feed,i,h}$ [kmol/s] denotes the molar flow rates of component i in the feed streams to the WGS 1 reactor in scenario h. For the methanation train, the extent of the WGS 1 reaction can be calculated using Equation 18.

$$\begin{gathered} f_{WGS1\_steam,\mathrm{H_2O},h} = \xi_{METHWGS,h}, \forall h \in \{1, ..., s\} \\ f_{WGS1\_feed,i,h} = f_{TMETH\_feed,i,h} + f_{WGS1\_steam,i,h}, \ \forall i \in I, \forall h \in \{1, ..., s\} \end{gathered} \tag{17}$$

$$\xi_{METHWGS,h} = \frac{f_{WGS1\_feed,\mathrm{CO},h} \cdot c_{SNGWGS,h}}{\nu_{CO,WGS}}, \forall h \in \{1, ..., s\} \tag{18}$$

Mass balance constraints of the form of Equation 19 are then implemented for the WGS 1 reactor where $f_{WGS1\_prod,i,h}$ [kmol/s] denotes the molar flow rates of component i in the product streams from the WGS 1 reactor in scenario h.

$$f_{WGS1\_prod,i,h} = f_{WGS1\_feed,i,h} + \nu_{i,WGS} \cdot \xi_{METHWGS,h}, \ \forall i \in I, \forall h \in \{1, ..., s\} \tag{19}$$

Syngas exiting the WGS 1 reactor then passes through a syngas cooler before heading to the CO_2 removal section.

Liquified (S)NG train - Selexol-based CO_2 removal

The cooled syngas stream heads to the Selexol 1 unit for CO_2 removal. The coefficients of separation for each relevant component i ($\beta_{SEL,i}$) are regressed from data generated from the Aspen HYSYS simulation presented in Table 11. Thus mass balances are implemented using Equation 20 with the clean tire-derived syngas sent to the downstream synthesis section. The terms $f_{METH\_in,i,h}$ and $f_{CO2\_rich1,i,h}$ [kmol/s] denote the molar flow rates of component i in the streams heading to the methanation reactor and the CO_2 rich stream from the Selexol 1 absorber respectively in scenario h.

Component, i	$\beta_{SEL,i}$
CO	6.970 E-4
CO_2	0.969
H_2	8.440 E-4
CH_4	8.200 E-5
H_2O	0.998
CH_3OH	5.026 E-3

Table 11: The coefficients of separation for each relevant component i in the CO_2 removal section.

$$f_{METH\_in,i,h} = (1.0 - \beta_{SEL,i}) \cdot f_{WGS1\_prod,i,h},\ \forall i \in I, \forall h \in \{1, ..., s\}$$
$$f_{CO2\_rich1,i,h} = \beta_{SEL,i} \cdot f_{WGS1\_prod,i,h},\ \forall i \in I, \forall h \in \{1, ..., s\} \tag{20}$$

Liquified (S)NG train - Methanation

The clean tire-derived syngas stream heads to a TREMP methanation process. Details of the process and the modeling strategy used are presented in our previous work ([3]) and in [36]. A constraint (Equation 21) is implemented to ensure that the tire-derived syngas composition heading to the methanation reactor has a feed gas module M_h equal to 3.0 in order to maximize methane production [59].

$$M_h = \frac{f_{METH\_in,\mathrm{H_2},h} - f_{METH\_in,\mathrm{CO_2},h}}{f_{METH\_in,\mathrm{CO},h} + f_{METH\_in,\mathrm{CO_2},h}} = 3.0, \forall h \in \{1, ..., s\} \tag{21}$$

The feed tire-derived syngas composition as well as all methanation operating conditions are fixed, thus the overall conversion is constant. For this reason, the production rate of methane (on a mass basis) in scenario h denoted by $m_{SNG,h}$ [kg/s] is implemented as a linear function (Equation 22) of the molar flow rate of relevant components in the syngas feed stream. The value of the coefficient β_{METH} is estimated from the Aspen Plus simulation to be 0.488.

$$m_{SNG,h} = \beta_{METH} \cdot (f_{METH\_in,\mathrm{CO},h} \cdot MW_{\mathrm{CO}} + f_{METH\_in,\mathrm{H_2},h} \cdot MW_{\mathrm{H_2}}, \forall h \in \{1, ..., s\}) \tag{22}$$

Liquified (S)NG train - Blending and Liquefaction

The SNG product derived from methanation of tire-derived syngas is first mixed with the corresponding (well) natural gas branch according to Equation 23, where $m_{ToLNG,h}$ is the mass of the mixed stream heading to the liquefaction unit in scenario h.

$$m_{ToLNG,h} = m_{SNG,h} + m_{NGLiq,h}, \forall h \in \{1, ..., s\} \tag{23}$$

The mixed natural gas stream is then passed through a molecular sieve in order to remove any remaining water to sub-ppm levels and 98.5 vol% of CO_2. Molecular sieves are designed to separate molecules based on differences in polarity and molecular size as detailed in Ref. [60]. The stream is then compressed to 55 bar in order to satisfy specifications for the natural gas liquefaction process [34]. Mass balance is trivially satisified (Equation 24), where m_{LNG} is the mass of liquefied (synthetic or well) natural gas [kg/s].

$$m_{LNG,h} = m_{ToLNG,h}, \forall h \in \{1, ..., s\} \tag{24}$$

Methanol Train - Natural Gas Reforming

One of the three branches from the natural gas feed stream (of mass in scenario h of $m_{NGRef,h}$) heads to a methanol train. First, the natural gas stream heads to a block termed the "Aggregate Natural Gas Converter" which encompasses a preheater, pre-reformer, reformer, syngas scrubber and compressor. Detailed descriptions of these units and the simulation strategy are presented in our previous work [3, 4, 43]. The natural gas-derived syngas mole flow rate in scenario h ($f_{NGRefprod\_dry,i,h}$) is a linear function of $m_{NGRef,h}$ (Equation 25). The mole fraction of component i belonging to the component set I ($x_{NGRefprod\_dry,i}$) is regressed from the Aspen Plus simulation with the coefficients presented in Table 12. The term $\frac{R_{S\_NG}}{MW_{NGRefprod\_dry}}$ (where $MW_{NGRefprod\_dry}$ is the molecular weight of natural gas-derived syngas and R_{S_NG} is the ratio of the mass flow rates of clean natural gas derived-syngas to the mass flow rate of the relevant natural gas branch) is also determined from the simulation to be 0.196 [$\text{kmols}^{-1}_{NGRefprod\_dry}/\text{kgs}^{-1}_{NG}$].

$$f_{NGRefprod\_dry,i,h} = \frac{x_{NGRefprod\_dry,i} \cdot R_{S\_NG} \cdot m_{NGRef,h}}{MW_{NGRefprod\_dry}}, \ \forall i \in I, \forall h \in \{1, ..., s\} \tag{25}$$

Component, i	$x_{NGRefprod\_dry,i}$
CO	0.228
CO_2	0.082
H_2	0.684

Table 12: The mole fractions of each relevant component i in natural gas-derived syngas obtained from the rigorous Aspen Plus simulation

Methanol Train - Water Gas Shift 2

Following the corresponding branch from the tire-derived syngas, the mass balance equations for the methanol train are similar to the corresponding units in the methanation train. For completeness, the corresponding equations are presented below but a description is not provided.

Water Gas Shift:

$$\begin{gathered} f_{WGS2\_steam,\mathrm{H_2O},h} = \xi_{MEOHWGS,h}, \forall h \in \{1, ..., s\} \\ f_{WGS2\_feed,i,h} = f_{TMEOH\_feed,i,h} + f_{WGS2\_steam,i,h}, \ \forall i \in I, \forall h \in \{1, ..., s\} \end{gathered} \tag{26}$$

$$\xi_{MEOHWGS,h} = \frac{f_{WGS2\_feed,\mathrm{CO},h} \cdot c_{MeOHWGS,h}}{\nu_{CO,WGS}}, \forall h \in \{1, ..., s\} \tag{27}$$

$$f_{WGS2\_prod,i,h} = f_{WGS2\_feed,i,h} + \nu_{i,WGS} \cdot \xi_{MEOHWGS,h}, \ \forall i \in I, \forall h \in \{1, ..., s\} \tag{28}$$

Methanol Train - Syngas blending and Selexol-based CO_2 removal

The tire and natural-gas derived syngas streams are blended in the appropriate ratio for methanol synthesis (Equation 29), with $f_{MEOH\_Blended,i,h}$ [kmol/s] denoting the molar flow rate of component i in scenario h in the blended syngas stream heading to the methanol synthesis section.

$$f_{MEOH\_Blended,i,h} = f_{WGS2\_prod,i,h} + f_{NGRefprod\_dry,i,h},\ \forall i \in I, \forall h \in \{1, ..., s\} \tag{29}$$

The blended tire and natural gas-derived syngas stream then heads to a Selexol unit for CO_2 removal.

$$\begin{gathered} f_{MEOH\_in,i,h} = (1.0 - \beta_{SEL,i}) \cdot f_{MEOH\_Blended,i,h},\ \forall i \in I, \forall h \in \{1, ..., s\} \\ f_{CO2\_rich2,i,h} = \beta_{SEL,i} \cdot f_{MEOH\_Blended,i,h},\ \forall i \in I, \forall h \in \{1, ..., s\} \end{gathered} \tag{30}$$

Methanol Train - Methanol synthesis

The clean blended syngas stream heads to the methanol synthesis section. The process description and the modeling approach used is presented in [38, 61]. In order to maximize the production of methanol, a constraint on the H_2/CO ratio of the feed syngas composition is implemented (31).

$$\frac{f_{MEOH\_in,\mathrm{H_2},h}}{f_{MEOH\_in,\mathrm{CO},h}} = 2.0, \forall h \in \{1, ..., s\} \tag{31}$$

By-products consisting of higher alcohols and off-gases are sent to the gas turbine for combustion and additional electricity generation [1]. The raw methanol stream is purified to a specification of 99.5%. The feed syngas composition as well as all methanol synthesis operating conditions are fixed, thus the overall conversion is constant. For this reason, the production rate of methanol (on a mass basis) denoted by $m_{MeOH,h}$ [kg/s] is implemented as a linear function (Equation 32) of the molar flow rate of relevant components in the syngas feed stream. The value of the coefficient β_{MEOH} is estimated from the Aspen Plus simulation to be 0.870.

$$m_{MeOH,h} = \beta_{MEOH} \cdot (f_{MEOH\_in,\mathrm{CO},h} \cdot MW_{\mathrm{CO}} + f_{MEOH\_in,\mathrm{H_2},h} \cdot MW_{\mathrm{H_2}}), \forall h \in \{1, ..., s\} \tag{32}$$

The produced methanol product could be further processed to DME, olefins or sold as final product. The corresponding split fractions to each of these sections is given by $S_{DME,h}$, $S_{MTO,h}$ and $S_{MeOHProd,h}$ respectively, thus the mass balance constraints are presented in Equation 33, where $m_{MeOH\_ToDME,h}$, $m_{MeOH\_ToMTO,h}$ and $m_{MeOH\_prod,h}$ [kg/s] are the mass flow rates of methanol heading to the DME, MTO and product sections respectively in scenario h.

$$\begin{aligned} m_{MeOH\_ToDME,h} &= m_{MeOH,h} \cdot S_{DME,h}, \forall h \in \{1, ..., s\} \\ m_{MeOH\_ToMTO,h} &= m_{MeOH,h} \cdot S_{MTO,h}, \forall h \in \{1, ..., s\} \\ m_{MeOH\_prod,h} &= m_{MeOH,h} \cdot S_{MeOHProd,h}, \forall h \in \{1, ..., s\} \\ S_{DME,h} + S_{MTO,h} + S_{MeOHProd,h} &= 1.0, \forall h \in \{1, ..., s\} \end{aligned} \tag{33}$$

DME synthesis

The feed methanol stream is dehydrated to produce DME. The process description and modeling approach presented in [38, 62] is used and the DME is purified to a specification of 99.5 mol%. The feed composition as well as all operating conditions are fixed, thus the overall conversion is constant. For this reason, the production rate of DME (on a mass basis) denoted by $m_{DME,h}$ [kg/s] is implemented as a linear function (Equation 34) of the feed mass flow rate of methanol. The value of the coefficient β_{DME} is estimated from the Aspen Plus simulation to be 0.615.

$$m_{DME,h} = \beta_{DME} \cdot m_{MeOH\_ToDME,h}, \forall h \in \{1, ..., s\} \tag{34}$$

Methanol to Olefins (MTO)

The methanol stream is dehydrated to produce ethylene, propylene and other hydrocarbons. The process configuration and modeling approach presented in [40] is used. The olefin product is first sent to a DGA-based CO_2 absorber before heading to a de-ethanizer column to remove ethylene, ethane and other light gases from the propylene and heavier components. The lighter stream heads to a de-methanizer and finally a C2-splitter to yield pure ethylene with the rest of the off-gases sent to the gas turbine. The heavier components are sent to a de-propanizer to yield propylene with the off-gases sent to the gas turbine. The feed composition as well as all operating conditions of all units in the MTO process are fixed, thus the overall conversion is

constant. For this reason, the production rates of ethylene ($m_{ethylene,h}$) and propylene ($m_{propylene,h}$) [kg/s] are implemented as a linear functions (Equation 35) of the feed mass flow rate of methanol ($m_{MeOH\_ToMTO,h}$). The value of the coefficients $\beta_{ethylene}$ and $\beta_{propylene}$ are estimated from the Aspen Plus simulation to be 0.070 and 0.062 respectively. Similarly, the mass of CO_2 ($m_{MTO\_CO2,\mathrm{CO_2},h}$) [kg/s] produced in the MTO process scales linearly with the mass flow rate of the feed methanol stream, with the corresponding coefficient β_{MTO_CO2} estimated as 0.0035.

$$\begin{aligned} m_{ethylene,h} &= \beta_{ethylene} \cdot m_{MeOH\_ToMTO,h}, \forall h \in \{1, ..., s\} \\ m_{propylene,h} &= \beta_{propylene} \cdot m_{MeOH\_ToMTO,h}, \forall h \in \{1, ..., s\} \\ m_{MTO\_CO2,\mathrm{CO_2},h} &= \beta_{MTO\_CO2} \cdot m_{MeOH\_ToMTO,h}, \forall h \in \{1, ..., s\} \end{aligned} \tag{35}$$

Gas Turbine

The relevant branches of the waste-tired derived syngas and natural gas together with off-gases from methanol synthesis and the MTO processes heads to a gas turbine for electricity generation together with compressed air and nitrogen from the ASU as a diluent. The mass of CO_2 ($m_{Flue,\mathrm{CO_2},h}$) [kg/s] contained in the flue gas can be calculated by Equation 36, with the coefficients $\beta_{NGGT,\mathrm{CO_2}}$, $\beta_{METHoff,\mathrm{CO_2}}$, $\beta_{MTOoff,\mathrm{CO_2}}$ given by 2.680 [$\mathrm{kg_{CO_2}/kg}_{NG\_GT}$] 0.157 [$\mathrm{kg_{CO_2}/kg}_{MEOH\_in}$] and 0.320 [$\mathrm{kg_{CO_2}/kg}_{MeOH\_ToMTO}$] respectively.

$$\begin{aligned} m_{Flue,\mathrm{CO_2},h} = (&f_{TGT\_feed,\mathrm{CO},h} \cdot MW_{\mathrm{CO_2}} + f_{TGT\_feed,\mathrm{CO_2},h} \cdot MW_{\mathrm{CO_2}} + f_{TGT\_feed,\mathrm{CH_4},h} \cdot MW_{\mathrm{CO_2}}) \\ &+ \beta_{NGGT,\mathrm{CO_2}} \cdot m_{NGGT,h} + \beta_{METHoff,\mathrm{CO_2}} \cdot m_{MEOH\_in,h} + \beta_{MTOoff,\mathrm{CO_2}} \cdot m_{MeOH\_ToMTO,h} \\ &\forall h \in \{1, ..., s\} \end{aligned} \tag{36}$$

Air separation unit (ASU)

Oxygen of 99.5 mol% purity for the the gasification, reforming and Claus processes is supplied by an ASU which is modeled according to the approach detailed in [6]. The total mass of oxygen produced ($m_{ASU,\mathrm{O_2},h}$) [kg/s] is given by Equation 37, $m_{Claus\_oxy,h}$ denotes the total mass of oxygen fed to the Claus process. The oxygen to tire ratio R_{OT} and oxygen to natural gas ratio R_{ONG}

which were considered as decision variables in our previous works ([4, 43]) are fixed in this work to be 0.91 and 0.95 respectively).

$$m_{ASU,\mathrm{O_2},h} = m_{tire,h} \cdot R_{OT} + m_{NGRef,h} \cdot R_{ONG} + m_{Claus\_oxy,h}, \quad \forall h \in \{1, ..., s\} \quad (37)$$

DGA-based postcombustion CO_2 capture

The split fraction of flue gas exiting the HRSG that heads to the DGA section for postcombustion CO_2 capture is given by $S_{PostCCS,h}$ while the split fraction emitted is given by $S_{PostEm,h}$. Thus, the mass flow rate of CO_2 captured ($m_{DGA,\mathrm{CO_2},h}$ [kg/s]) is given by Equation 38, while $m_{GTEmitted,\mathrm{CO_2},h}$ [kg/s] denotes the mass of CO_2 in flue gas emitted. A CO_2 capture rate c_{CCS} of 0.90 is assumed.

$$\begin{gathered} m_{DGA,\mathrm{CO_2},h} = S_{PostCCS,h} \cdot m_{Flue,\mathrm{CO_2},h} \cdot c_{CCS}, \forall h \in \{1, ..., s\} \\ m_{GTEmitted,\mathrm{CO_2},h} = S_{PostEm,h} \cdot m_{Flue,\mathrm{CO_2},h} + (1.0 - c_{CCS}) \cdot S_{PostCCS,h} \cdot m_{Flue,\mathrm{CO_2},h}, \\ \forall h \in \{1, ..., s\}, \\ S_{PostCCS,h} + S_{PostEm,h} = 1.0, \forall h \in \{1, ..., s\} \end{gathered} \quad (38)$$

CO_2 compression, liquefaction & sequestration

The mass of CO_2 removed in the Selexol 1, Selexol 2 and MTO processes in scenario h ($m_{Pre,\mathrm{CO_2},h}$ [kg/s]) is calculated using Equation 39. The split fraction of CO_2 removed in these three sections sent to sequestration ($S_{PreCCS,h}$) determines the mass flow rate of CO_2 sequestered ($m_{PreCCS,h}$) and emitted ($m_{PreEmitted,h}$) [kg/s]. The corresponding split fraction emitted is denoted $S_{PreEm,h}$.

$$m_{Pre,\mathrm{CO_2},h} = f_{CO2\_rich1,\mathrm{CO_2},h} \cdot MW_{\mathrm{CO_2}} + f_{CO2\_rich2,\mathrm{CO_2},h} \cdot MW_{\mathrm{CO_2}} + m_{MTO\_CO2,\mathrm{CO_2},h}, \forall h \in \{1, ..., s\},$$
$$m_{PreCCS,h} = S_{PreCCS,h} \cdot m_{Pre,\mathrm{CO_2},h}, \forall h \in \{1, ..., s\}$$
$$m_{PreEmitted,h} = S_{PreEm,h} \cdot m_{Pre,\mathrm{CO_2},h}, \forall h \in \{1, ..., s\}$$
$$S_{PreCCS,h} + S_{PreEm,h} = 1.0, , \forall h \in \{1, ..., s\} \tag{39}$$

The total amount of $\mathrm{CO_2}$ sequestered ($m_{CCS,\mathrm{CO_2},h}$) and emitted ($m_{Emitted,\mathrm{CO_2},h}$) [kg/s] is given by Equations 40 and 41 respectively.

$$m_{CCS,\mathrm{CO_2},h} = m_{PreCCS,h} + m_{DGA,\mathrm{CO_2},h}, \forall h \in \{1, ..., s\} \tag{40}$$

$$m_{Emitted,\mathrm{CO_2},h} = m_{GTEmitted,\mathrm{CO_2},h} + m_{PreEmitted,h}, \forall h \in \{1, ..., s\} \tag{41}$$

Energy balance models

For each section $u \in U$ listed in Table 6, the utility requirements in scenario h are divided into low quality heat ($Q_{LQ,u,h}$), high quality heat ($Q_{HQ,u,h}$), cooling water ($Q_{CW,u,h}$) and electricity ($W_{u,h}$) all in [MW]. Similar to the approach of Chen et al. [41], heat sources available at temperatures above 220 °C are considered high quality while all other sources are considered low quality. $Q_{HQ,u,h}$ and $Q_{LQ,u,h}$ are positive if the corresponding section generates net heat and negative if it consumes heat.

Gas Turbine

The total thermal input (on a LHV basis) to the gas turbine in scenario h denoted $Q_{GTin,h}$ [MW] is given by Equation 42, where $Q_{GTin,TDsyngas,h}$, $Q_{GTin,NGGT,h}$, $Q_{GTin,METHoff,h}$, $Q_{GTin,DMEoff,h}$, $Q_{GTin,MTOoff,h}$ denote the contributions arising from the relevant tire-derived syngas branch, natural gas branch, methanol synthesis offgases, DME synthesis offgases and MTO offgases respectively. The values of $\beta_{METHoff} \cdot LHV_{METHoff}$, $\beta_{DMEoff} \cdot LHV_{DMEoff}$, and $\beta_{MTOoff} \cdot LHV_{MTOoff}$ are 2.602 [MJ/kg$_{MEOH_in}$], 0.023 [MJ/kg$_{MeOH_ToDME}$] and 1.854 [MJ/kg$_{MeOH_ToMTO}$] respectively.

$$
\begin{aligned}
Q_{GTin,TDsyngas,h} = f_{TGT\_feed,\mathrm{CO},h} \cdot MW_{\mathrm{CO}} \cdot LHV_{\mathrm{CO}} + f_{TGT\_feed,\mathrm{H_2},h} \cdot MW_{\mathrm{H_2}} \cdot LHV_{\mathrm{H_2}} \\
+ f_{TGT\_feed,\mathrm{CH_4},h} \cdot MW_{\mathrm{CH_4}} \cdot LHV_{\mathrm{CH_4}}, \forall h \in \{1, ..., s\} \\
Q_{GTin,NGGT,h} = m_{NGGT,h} \cdot LHV_{NG}, , \forall h \in \{1, ..., s\} \\
Q_{GTin,METHoff,h} = \beta_{METHoff} \cdot m_{MEOH\_in,h} \cdot LHV_{METHoff}, \forall h \in \{1, ..., s\} \\
Q_{GTin,DMEoff,h} = \beta_{DMEoff} \cdot m_{MeOH\_ToDME,h} \cdot LHV_{DMEoff}, \forall h \in \{1, ..., s\} \\
Q_{GTin,MTOoff,h} = \beta_{MTOoff} \cdot m_{MeOH\_ToMTO,h} \cdot LHV_{MTOoff}, \forall h \in \{1, ..., s\} \\
Q_{GTin,h} = Q_{GTin,TDsyngas,h} + Q_{GTin,NGGT,h} + Q_{GTin,METHoff,h} \\
+ Q_{GTin,DMEoff,h} + Q_{GTin,MTOoff,h}, \forall h \in \{1, ..., s\}
\end{aligned}
\tag{42}
$$

The electricity generated by the gas turbine in scenario h ($W_{GT,h}$ [MW]) is calculated using Equation 43; the gas turbine efficiency (η_{GT}) is given by 0.468 as suggested by Chen et al. [42, 41].

$$
W_{GT,h} = \eta_{GT} \cdot Q_{GTin,h}, \forall h \in \{1, ..., s\} \tag{43}
$$

The flue gas from the gas turbine then heads to a HRSG system for additional heat recovery.

Heat Recovery Steam Generator (HRSG)

The amount of high quality heat recovered in the HRSG in scenario h ($Q_{HQ\_HRSG,h}$ [MW]) from flue gases exiting the gas turbine is expressed as a linear function of the net work generated in the gas turbine as presented in Equation 44, where the coefficient β_{HQ_HRSG} is estimated from the Aspen Plus model to be 1.1272 [$\mathrm{MW}_{heat,HRSG}/\mathrm{MW}_{work,GT}$].

$$
Q_{HQ\_HRSG,h} = \beta_{HQ\_HRSG} \cdot W_{GT,h}, \forall h \in \{1, ..., s\} \tag{44}
$$

Other Sections

For all other sections, we assume that the $Q_{LQ,u,h}$, $Q_{HQ,u,h}$, $Q_{CW,u,h}$ and $W_{u,h}$ values can be approximated by linear function of the characteristic throughput ($F_{u,h}$ in Table 6). This is presented in Equations 45, 46, 47 and 48 respectively with the coefficients $\beta_{HQ,u}$, $\beta_{LQ,u}$, $\beta_{CW,u}$ and $\beta_{W,u}$ presented in Table 13.

$$Q_{HQ,u,h} = \beta_{HQ,u} \cdot F_{u,h}, \forall h \in \{1, ..., s\} \tag{45}$$

$$Q_{LQ,u,h} = \beta_{LQ,u} \cdot F_{u,h}, \forall h \in \{1, ..., s\} \tag{46}$$

$$Q_{CW,u,h} = \beta_{CW,u} \cdot F_{u,h}, \forall h \in \{1, ..., s\} \tag{47}$$

$$W_{u,h} = \beta_{W,u} \cdot F_{u,h}, \forall h \in \{1, ..., s\} \tag{48}$$

The total amount of cooling water required in scenario h ($Q_{CW\_net,h}$) [MW] is given by Equation 49

$$Q_{CW\_net,h} = \sum_{u \in U} Q_{CW,u,h}, \forall h \in \{1, ..., s\} \tag{49}$$

	Process Section, u	$\beta_{HQ,u}$	$\beta_{LQ,u}$	$\beta_{CW,u}$	$\beta_{W,u}$
			$[\text{MW}.F_{u,h}^{-1}]$		
	Waste Tire Train				
1.	Aggregate Waste Tire converter	2.183	-0.438	4.973	-0.074
2.	Air Separation Unit	0.0	0.0	0.0	-1.4760
	Product train - (Synthetic) Natural gas				
3.	SNG train - Water Gas Shift 1	-25.6167	-38.9110	0.0	-0.4256
4.	SNG train - Selexol 1 CO_2 removal	0.0	0.0	4.4668	-4.3947
5.	Methanation	6.0058	0.3216	0.9088	0.0
6.	(Synthetic or well) NG Liquefaction	0.0	0.0	0.0	-1.0042
7.	Aggregate Natural gas converter	1.9190	0.0	5.0035	-2.4156
	Product train - Methanol, DME and olefins				
8.	MeOH train -Water Gas Shift 2	-25.6167	-38.9110	0.0	-0.4256
9.	MeOH train - Selexol 2 CO_2 removal	0.0	0.0	4.4668	-4.3947
10.	Methanol synthesis & purification	0.0	-0.3999	4.0337	-0.0071
11.	DME synthesis	0.0	-0.5425	1.7579	-0.0095
12.	Methanol to Olefins	0.0	-0.1703	0.9674	-0.0556
	Product train - Power generation				
13.	Gas Turbine	0.0	0.0	0.0	0.0
14.	HRSG	0.0	0.0	0.0	0.0
15.	Steam Turbine	0.0	0.0	0.0	0.0
16.	Electric Plant Accessories	0.0	0.0	0.0	0.0
	CO_2 capture and miscellaneous				
17.	DGA CO_2 removal	0.0	-6.2315	1.8839	-0.0339
18.	CO_2 compression, liquefaction & sequestration	0.0	0.0	0.4076	-0.0977
19.	Miscellaneous	0.0	0.0	0.0	0.0
20.	Water systems	0.0	0.0	0.0	0.0

Table 13: Coefficients for utility consumption calculations for relevant process sections

Steam Turbine

The excess high quality ($Q_{HQ\_net,h}$) and low quality heat ($Q_{LQ\_net,h}$) in scenario h [MW] is given by Equations 50 and 51 respectively.

$$Q_{HQ\_net,h} = \sum_{u \in U} Q_{HQ,u,h}, \forall h \in \{1, ..., s\} \tag{50}$$

$$Q_{LQ\_net,h} = \sum_{u \in U} Q_{LQ,u,h}, \forall h \in \{1, ..., s\} \tag{51}$$

This excess heat is used to generate steam which then produces work in the steam turbine ($W_{ST,h}$) as presented in Equation 52, with the efficiency of conversion of high quality ($\eta_{ST,HQ}$) and low quality heat ($\eta_{ST,LQ}$) given by 0.4407 and 0.1542 respectively as determined in [41].

$$W_{ST,h} = \eta_{ST,HQ} \cdot Q_{HQ\_net,h} + \eta_{ST,LQ} \cdot Q_{LQ\_net,h}, \forall h \in \{1, ..., s\} \tag{52}$$

The net work in scenario h ($W_{net,h}$ [MW]) generated by the polygeneration system is given by Equation 53.

$$W_{net,h} = W_{ST,h} + W_{GT,h} - \sum_{u \in U \setminus \{GT,ST\}} \beta_{W,u} \cdot F_{u,h}, \forall h \in \{1, ..., s\} \tag{53}$$

Scale constraint

In order to keep the designed polygeneration system comparable with previous work ([3, 44]), we constrain the total thermal input in any scenario h ($TI_{LHV,h}$) to be less than 893 MW as illustrated in Equation 54.

$$TI_{LHV,h} = m_{tire,h} \cdot LHV_{tire} + m_{NG,h} \cdot LHV_{NG} \leq 893, \quad [\text{MW}] \quad \forall h \in \{1, ..., s\} \tag{54}$$

Annual Operating Cost model

These can be subdivided into variable and fixed operating cost.

Variable Operating Cost

Variable operating costs for the different sections include feedstock costs (other than waste tire and natural gas), solvent and catalyst costs as well as waste disposal costs. In this work, we assume that these costs can be approximated by linear functions of the characteristic throughput ($F_{u,h}$ in Table 6). Thus, the total variable annual operating cost in scenario h ($OPEX_{var,h}$ in [M$\$_{2018}$/yr]) is given by Equation 55, where the coefficients $OPEX_{var,u}$ are presented in Table 14 for relevant sections. The parameter P_{CW} denotes the cost of cooling water estimated to be 1.407E-4 [M$\$_{2018} \cdot \text{yr}^{-1} \cdot \text{MW}^{-1}$] [3]. We note that all costs are scaled to $\$_{2018}$ assuming a yearly inflation rate of 2.75%.

$$OPEX_{var,h} = (\sum_{u \in U} OPEX_{var,u} \cdot F_{u,h}) + P_{CW} \cdot Q_{CW\_net,h}, \forall h \in \{1, ..., s\} \quad (55)$$

	Process Section, u	**Feedstock cost**	**Solvent cost**	**Catalyst cost** $[\$_{2018} \cdot \mathrm{yr}^{-1} F_{u,h}^{-1}]$	**Waste costs**	**Total** ($OPEX_{var,u}$)	Remarks
	Waste Tire Train						
1.	Aggregate Waste Tire converter	7,125	898	5,229	29,220	42,472.16	Water makeup, Ash handling, sulfur removal, catalyst [43]
2.	Air Separation Unit	0	0	0	0	0	-
	Product train - (Synthetic) Natural gas						
3.	SNG train - Water Gas Shift 1	404,892	0	375,683	0	780,575	Catalyst and feed water cost [31]
4.	SNG train - Selexol 1 CO_2 removal	0	91,074	0	0	91,074	Solvent make up costs [31, 1]
5.	Methanation	0	0	18,652	11,422	30,075	Catalyst and waste water treatment [63, 3]
6.	(Synthetic or well) NG Liquefaction	0	0	0	0	0	0
7.	Aggregate Natural gas converter	1,484	0	88,908	0	90,392	Steam feed and catalyst costs [6]
	Product train - Methanol, DME and olefins						
8.	MeOH train -Water Gas Shift 2	404,892	0	375,683	0	780,575	Catalyst and feed water cost [31]
9.	MeOH train - Selexol 2 CO_2 removal	0	91,074	0	0	91,074	Solvent make up costs [31, 1]
10.	Methanol synthesis & purification	0	0	0	5,279	5,279	Waste water treatment
11.	DME synthesis	0	0	0	0	0	-
12.	Methanol to Olefins	4,174	0	0	29,236	33,410	Feed and waste water costs [40]
	Product train - Power generation						
13.	Gas Turbine	0	0	0	0	0	0
14.	HRSG	0	0	0	0	0	0
15.	Steam Turbine	0	0	0	0	0	0
16.	Electric Plant Accessories	0	0	0	0	0	0
	CO_2 capture and miscellaneous						
17.	DGA CO_2 removal	0	5,158	0	0	5,158	Solvent make up costs [3]
18.	CO_2 compression, liquefaction & sequestration	0	0	0	295,478	295,478	Transportation & sequestration costs [1]
19.	Miscellaneous	0	0	0	0	0	0
20.	Water systems	0	0	0	0	0	0

Table 14: Variable operating costs for the different sections including feedstock, solvent, catalyst and waste disposal costs.

Fixed Operating Costs

Fixed operating costs include labor costs (operating and maintenance labor), operating overhead and property taxes and insurance. We assume that annual fixed operating costs in scenario h ($OPEX_{fixed,h}$ in [M$\$_{2018}$/yr]) scale linearly with the plants total thermal input ($TI_{LHV,h}$) as presented in Equation 56, where the coefficient $OPEX_{fixed,0}$ is estimated from Woods et al. [31] to be 5,114 $\$_{2018}\cdot\text{yr}^{-1}\cdot\text{MW}^{-1}$ (scaled to $\$_{2018}$ assuming a yearly inflation rate of 2.75%).

$$OPEX_{fixed,h} = OPEX_{fixed,0} \cdot TI_{LHV,h}, \forall h \in \{1, ..., s\} \tag{56}$$

Capital cost model

Each process section/piece of equipment can take on only one size from a discrete set of equipment sizes. The discrete set of equipment sizes is generated according to the approach of Chen et al. [19] as presented in Equation 57, where $S_{u,j}$ is the j^{th} choice of size of equipment u, S_u^{LBD} and S_u^{UBD} are the lower and upper bounds on the size of equipment u (presented in Table 15), and d is the number of equipment sizes available (i.e., the cardinality of the discrete set of sizes) which is set to be 10 to keep the problem tractable for global optimization solvers. We note that the lower bound of capacity (S_u^{LBD}) is taken to 0.0 for all sections.

$$S_{u,j} = S_u^{LBD} + \frac{j-1}{d-1} \cdot (S_u^{UBD} - S_u^{LBD}),\ \forall u \in U,\ \forall j \in \{1, ..., d\} \tag{57}$$

The capital cost associated with each $S_{u,j}$ ($Cap_{u,j}$ [M$\$_{2018}$]) is given by Equation 58, where $Cap_{u,0}$, $S_{u,0}$ and sf_u denote the base cost, base capacity and scaling factor of section u (presented in Table 15). All costs are scaled to $\$_{2018}$ using the CEPCI index method.

$$Cap_{u,j} = Cap_{u,0} \cdot \left(\frac{S_{u,j}}{S_{u,0}}\right)^{sf_u},\ \forall u \in U,\ \forall j \in \{1, ..., d\} \tag{58}$$

For each section u, a binary decision variable $y_{u,j}$ denotes whether the j^{th} choice for its size is selected or not, and $\mathbf{y}$ denotes a vector of these binary decision variables. Equation 59 represents the constraint that only one size can be selected.

$$\sum_{j=1}^{d} y_{u,j} = 1, \ \forall u \in U \tag{59}$$

The actual (designed) equipment size (S_u) and corresponding capital cost of each section (Cap_u [M$\$_{2018}$]) thus can be expressed as a function of the binary decision variables as presented in Equations 60 and 61 respectively. The characteristic throughput value ($F_{u,h}$) through each process section in any scenario h is constrained to be lower than the section's capacity (Equation 63). We note that these constraints are linking (complicating) constraints as they link first-stage and second-stage variables.

$$S_u = \sum_{j=1}^{d} S_{u,j} \cdot y_{u,j}, \ \forall u \in U \tag{60}$$

$$Cap_u = \sum_{j=1}^{d} Cap_{u,j} \cdot y_{u,j}, \ \forall u \in U \tag{61}$$

The total capital cost of the polygeneration system (Cap [M$\$_{2018}$]) is given by Equation 62, where K_L and K_{WC} are factors representing the additional costs associated with purchasing land and working capital (set at 2.0% and 5.0% respectively of the total equipment cost).

$$Cap = (K_L + K_{WC}) \cdot \sum_{u \in U} Cap_u \tag{62}$$

$$F_{u,h} \leq S_u, \ \forall u \in U, \forall h \in \{1, ..., s\} \tag{63}$$

	Process Section, u	**Ref. cost** ($Cap_{u,0}$) [M$]	**Ref. Capacity** ($S_{u,0}$)	**Max. Capacity** (S_u^{UBD}) [1]	**Units**	**Scaling factor**	**Year**	**Ref**
	Waste Tire Train							
1.	Aggregate Waste Tire converter	492.0	61.4	30.0	kg/s tire	0.7	2007	[43]
2.	Air Separation Unit	250.8 [2]	49.4	50.0	kg/s O_2	0.7	2007	[31, 64]
	Product train - (Synthetic) Natural gas							
3.	SNG train - Water Gas Shift 1	20.8	2.236	5.0	kmol/s CO	0.7	2007	[31]
4.	SNG train - Selexol 1 CO_2 removal	61.5	3.241	3.0	kmol/s CO_2	0.7	2010	[1, 65, 66]
5.	Methanation	93.6	90.9	90.0	kg/s syngas	0.6	2007	[63], APEA
6.	(Synthetic or well) NG Liquefaction	20.5	9.7	30.0	kg/s SNG	0.6	2018	[3], APEA
7.	Aggregate Natural gas converter	53.7	18.1	25.0	kg/s natural gas	0.6	2017	[6]
	Product train - Methanol, DME and olefins							
8.	MeOH train -Water Gas Shift 2	20.8	2.236	5.0	kmol/s CO	0.7	2007	[31]
9.	MeOH train - Selexol 2 CO_2 removal	61.5	3.241	3.0	kmol/s CO_2	0.7	2010	[1, 65, 66]
10.	Methanol synthesis & purification	91.7	90.0	120.0	kg/s syngas	0.65	2003	[67]
11.	DME synthesis	34.0	11.0	35.0	kg/s MeOH	0.65	2003	[68]
12.	Methanol to Olefins	330.1	62.5	35.0	kg/s MeOH	0.60	2012	[69]
	Product train - Power generation							
13.	Gas Turbine	140.2	464	550.0	MW	0.7	2007	[31]
14.	HRSG	57.6	522.9	600.0	MW	0.7	2007	[31]
15.	Steam Turbine	63.6	263.5	500.0	MW	0.7	2007	[31]
16.	Electric Plant Accessories	89.5	734.0	900.0	MW	0.6	2007	[31]
	CO_2 capture and miscellaneous							
17.	DGA CO_2 removal	48.2	21.9	80.0	kg/s CO_2	0.6	2016	APEA
18.	CO_2 compression, liquefaction & sequestration	7.8	43.2	80.0	kg/s CO_2	0.6	2018	[3]
19.	Miscellaneous	58.1	893	893	MW LHV	0.6	2018	[3], APEA
20.	Water systems	75.6	419.2	800.0	MW	0.7	2007	[31]

Table 15: Reference capital cost data for the different sections. The reference rate corresponds to the same material or energy stream as the characteristic throughput $F_{u,h}$ in Table 6. [1] We note that the maximum capacity ($S_{u,0}$) is tightened to the scale of the process studied. [2] An additional 5.0% is added to the reference cost of [31] to account for the higher O_2 purity of 99.5% used [64]. APEA denotes Aspen Process Economic Analyzer.

Feed and Product Prices & CO_2 tax rates

The main text presents the feed and product prices & CO_2 tax rates used in the economic analysis.

Annual Net Profit Calculation

The annual revenues obtained from product sales in scenario h ($Rev_{Annual,h}$ [M$\$_{2018}$.yr^{-1}]) is given by Equation 64, where $k_{LNG,NG}$ is a factor that accounts for the price premium of liquefied SNG compared to SNG (equal to 1.65) and P_{Sulfur} is the price of sulfur (equal to 0.11 [\$/kg]), and t_{op} is the annual plant operating time (equal to 7,446 hours, assuming 85% availability).

$$\begin{aligned} Rev_{Annual,h} = \frac{t_{op}}{1E6} \cdot (k_{LNG,NG} \cdot P_{NG,h} \cdot m_{LNG,h} + P_{Elec,h} \cdot W_{net,h} + P_{MeOH,h} \cdot m_{MeOH,h} \\ + P_{DME,h} \cdot m_{DME,h} + P_{Ethylene,h} \cdot m_{ethylene,h} + P_{Propylene,h} \cdot m_{propylene,h} + \\ P_{Sulfur} \cdot m_{CLAUS,\mathrm{S},h} - P_{\mathrm{CO_2},h} \cdot m_{Emitted,\mathrm{CO_2},h}), \\ \forall h \in \{1, ..., s\} \end{aligned} \tag{64}$$

The annual tire and natural gas feedstock cost in scenario h ($Feed_{Annual}$ [M$\$_{2018}$/yr]) is given by Equation 65.

$$\begin{aligned} Feed_{Annual,h} = \frac{t_{op}}{1E6} \cdot (P_{Tire,h} \cdot m_{tire,h} + P_{NG,h} \cdot m_{NG,h}) \\ \forall h \in \{1, ..., s\} \end{aligned} \tag{65}$$

The annual net profit in scenario h ($Pro_{net,h}$ [M$\$_{2018}$/yr]) is given by Equation 66, where R_{tax} denotes the tax rate presented in Table 16.

$$\begin{aligned} Pro_{net,h} = (1.0 - R_{tax}) \cdot (Rev_{Annual,h} - Feed_{Annual,h} - OPEX_{var,h} - OPEX_{fixed,h}), \\ \forall h \in \{1, ..., s\} \end{aligned} \tag{66}$$

Reformulation-Linearization Technique (RLT) constraints

As discussed in the main text, the following RLT equations are implemented to yield tighter convex relaxations for constraints given by Equations 14, 15, 33, 38, 39 respectively.

$$f_{TDsweet\_gas,i,h} = f_{TMETH\_feed,i,h} + f_{TGT\_feed,i,h} + f_{TMEOH\_feed,i,h}, \quad \forall i \in I, \forall h \in \{1, ..., s\} \tag{67}$$

$$m_{NG,h} = m_{NGRef,h} + m_{NGGT,h} + m_{NGLiq,h}, \forall h \in \{1, ..., s\} \tag{68}$$

$$m_{MeOH,h} = m_{MeOH\_ToDME,h} + m_{MeOH\_ToMTO,h} + m_{MeOH\_prod,h}, \forall h \in \{1, ..., s\} \tag{69}$$

$$m_{Flue,\mathrm{CO_2},h} = m_{DGA,\mathrm{CO_2},h} + m_{GTEmitted,\mathrm{CO_2},h}, \forall h \in \{1, ..., s\} \tag{70}$$

$$m_{Pre,\mathrm{CO_2},h} = m_{PreCCS,h} + m_{PreEmitted,h}, \forall h \in \{1, ..., s\} \tag{71}$$

Optimization Problem Formulation

The optimal design and operation problem is formulated as a nonconvex two-stage stochastic MINLP (Equation FP) where the expected Net Present Value (NPV) is used as the objective function. The annual discount rate (r), depreciation time (t_{dp}), project lifetime (t_{lf}) are presented in Table 16.

$$\max_{\mathbf{y},\mathbf{x}_1,\ldots,\mathbf{x}_s} \quad \mathbb{E}_{\boldsymbol{\omega}}[\text{NPV}] = Cap(\mathbf{y}) \cdot \Big[-1 + \frac{R_{tax}}{r \cdot t_{dp}} \cdot \Big(1 - \frac{1}{(1+r)^{t_{dp}}}\Big)\Big]$$
$$+ \sum_{h=1}^{s} p_h \cdot Pro_{net,h}(\mathbf{x}_h, \boldsymbol{\omega}_h) \cdot \Big[\frac{1}{r} \cdot \Big(1 - \frac{1}{(1+r)^{t_{lf}}}\Big)\Big]$$

s.t. First-stage constraints: Capital cost model [Equations 57 - 62],

Second-stage constraints: Mass balance model [Equations 12 - 41]

Energy balance model [Equations 42- 53]

Operating cost model [Equations 55 - 56]

Annual net profit model [Equations 64 - 66]

Scale constraint [Equations 54]

RLT constraints [Equations 67 - 71]

Linking constraints: Throughput$_h \leq$ Equipment Capacity [Equations 63]

(FP)

Parameter	**Value**	**Ref**
Base Year	2018	
Plant lifetime (t_{lf})	30 yrs	[70, 1]
Working capital	5.0 % TPC [1]	[71, 6]
Land	2.0 % TPC [1]	[6]
Annual discount rate (r)	20 %	[72]
Income Tax Rate (R_{tax})	40.0 %	[70, 1]
Depreciation period (t_{dp})	10 years	[1]
Capacity factor	85%	[1]

Table 16: Assumed economic parameters for calculation of NPV.

Scenario generation for computational studies

The number of scenarios considered for each uncertain parameter in the computational study of Figure 2 in the main text is presented in Table 17. The approach presented in Li et al. [12] is used to generate the scenario tree.

s	$P_{NG,h}$	$P_{Elec,h}$	$P_{MeOH,h}$	$P_{DME,h}$	$P_{Ethylene,h}$	$P_{Propylene,h}$	$P_{Tire,h}$	$P_{\mathrm{CO_2},h}$
2	1	2	1	1	1	1	1	1
4	1	2	2	1	1	1	1	1
8	1	2	2	1	1	1	2	1
16	2	2	2	1	1	1	2	1
32	2	2	2	2	1	1	2	1
64	2	2	2	2	1	1	2	2
128	2	2	2	2	2	1	2	2
256	2	2	2	2	2	2	2	2
384	2	3	2	2	2	2	2	2
576	2	3	3	2	2	2	2	2
864	2	3	3	2	2	2	3	2

Table 17: Number of scenarios considered for each uncertain parameter in the computational study of Figure 2 in the main text